

# Detailing Cloud Property Feedbacks with a Regime-Based Decomposition

Mark Zelinka (✉ [zelinka1@llnl.gov](mailto:zelinka1@llnl.gov))

LLNL: Lawrence Livermore National Laboratory <https://orcid.org/0000-0002-6570-5445>

Ivy Tan

McGill University

Lazaros Oreopoulos

NASA Goddard Space Flight Center

George Tselioudis

NASA

---

## Research Article

**Keywords:** climate sensitivity, cloud feedback, cloud regimes

**Posted Date:** April 26th, 2022

**DOI:** <https://doi.org/10.21203/rs.3.rs-1562696/v1>

**License:**  This work is licensed under a Creative Commons Attribution 4.0 International License.

[Read Full License](#)

---

## Detailing Cloud Property Feedbacks with a Regime-Based Decomposition

Mark D. Zelinka · Ivy Tan · Lazaros  
Oreopoulos · George Tselioudis

Received: date / Accepted: date

1 **Abstract** Diagnosing the root causes of cloud feedback in climate models and  
2 reasons for inter-model disagreement is a necessary first step in understanding  
3 their wide variation in climate sensitivities. Here we bring together two anal-  
4 ysis techniques that illuminate complementary aspects of cloud feedback. The  
5 first quantifies feedbacks from changes in cloud amount, altitude, and optical  
6 depth, while the second separates feedbacks due to cloud property changes  
7 within specific cloud regimes from those due to regime occurrence frequency  
8 changes. We find that in the global mean, shortwave cloud feedback averaged  
9 across ten models comes solely from a positive within-regime cloud amount  
10 feedback countered slightly by a negative within-regime optical depth feed-  
11 back. These within-regime feedbacks are highly uniform: In nearly all regimes,  
12 locations, and models, cloud amount decreases and cloud albedo increases with  
13 warming. In contrast, between-regime components vary widely across models  
14 but are very small on average. This component, however, is dominant in set-

---

M. Zelinka  
Lawrence Livermore National Laboratory  
7000 East Avenue, L-103  
Livermore, CA 94550, USA  
E-mail: zelinka1@llnl.gov

I. Tan  
McGill University  
Room 817, Burnside Hall  
805 Sherbrooke Street West  
Montreal, Quebec, H3A 0B9, Canada

L. Oreopoulos  
NASA/GSFC  
Mail Code: 613  
Greenbelt, MD 20771, USA

G. Tselioudis  
NASA Goddard Institute for Space Studies  
2880 Broadway  
New York, NY 10025, USA

ting the geographic structure of the shortwave cloud feedback: Thicker, more extensive cloud types increase at the expense of thinner, less extensive cloud types in the extratropics, and vice versa at low latitudes. The prominent negative extratropical optical depth feedback has contributions from both within- and between-regime components, suggesting that thermodynamic processes affecting cloud properties as well as dynamical processes that favor thicker cloud regimes are important. The feedback breakdown presented herein may provide additional targets for observational constraints by isolating cloud property feedbacks within specific regimes without the obfuscating effects of changing dynamics that may differ across timescales.

**Keywords** climate sensitivity · cloud feedback · cloud regimes

## 1 Introduction

The responses of clouds to planetary warming – cloud feedbacks – are the primary cause of uncertainties in future warming for a given increase in greenhouse gas concentration. This stems from the large role of clouds in modifying the flow of heat into and out of the Earth system and the challenge of observing, understanding, and modeling cloud processes at scales ranging from microscopic to global for the wide variety of cloud types and responses to warming that together make up the cloud feedback.

Recent work using cloud radiative kernels (Zelinka et al, 2012a,b, 2013, 2016) has advanced our ability to diagnose cloud feedbacks, providing new insights into robust features simulated by all models, their linkage to the physical processes driving them, and their sources of inter-model spread. For example, it is now clear that models systematically simulate positive feedbacks from decreases in low-cloud amount, positive feedbacks from rising high-cloud top altitude, and negative feedbacks from increases in low-cloud optical depth.

However, as noted in Zelinka et al (2012a), there remains ambiguity regarding the actual causes of the cloud changes that drive some of these components. For example, climate models robustly simulate a negative feedback from increased optical depth of (primarily) low-level extratropical clouds. This feedback could have contributions from both changes in the relative frequency of occurrence of optically thin versus thick cloud types as well as from changes in the optical properties of clouds of a given morphology. In the former case, it is possible that transitions from relatively thin boundary layer clouds to thicker frontal clouds, perhaps associated with a storm-track shift, are leading to the overall increase in cloud albedo. This would imply that a better understanding of changes in meteorology and large-scale dynamics would be necessary to constrain this feedback. In the latter case, optical properties of the cloud types that are already present are changing (e.g., thin boundary layer clouds becoming thicker), suggesting a greater role for thermodynamic processes that increase cloud liquid water content or decrease particle size. While it is likely that some combination of both processes contributes to this and other feedbacks, distinguishing the two would be helpful for interpreting

which processes drive the feedback on average, which drive its inter-model spread, and which processes need attention when determining how to correct biases in models.

Independent of the work done using cloud radiative kernels, novel techniques have allowed for a clear breakdown of cloud feedbacks into components due to changes in the relative frequency of occurrence of various cloud regimes and due to changes in within-regime cloud radiative properties (Williams and Tselioudis, 2007; Williams and Webb, 2009; Tsushima et al, 2016). These are related to and build on previous work separating tropical cloud regimes into vertical motion regimes, allowing for a clean separation of thermodynamic (within-regime) and dynamic (between-regime) components of cloud feedback (Bony et al, 2004; Bony and Dufresne, 2005; Bony et al, 1997). These analyses typically rely on cloud radiative effect (CRE; the difference between clear- and all-sky top of atmosphere radiative fluxes) — a useful but highly integrated measure of how clouds impact radiation. As such, results derived therein do not distinguish changes in, for example, cloud altitude from cloud amount in driving longwave CRE changes in a given regime, or between cloud amount and cloud optical depth in driving shortwave CRE changes in a given regime. It is also unclear how between-regime changes manifest in cloud property feedbacks (e.g., how population shifts between cloud regimes with distinct radiative properties translate into amount, altitude, and optical depth feedbacks).

Hence it is natural to bring together these two techniques to leverage their strengths in detailing complementary aspects of cloud feedback. Cloud regime analysis would illuminate the currently ambiguous processes driving some of the robust yet uncertain cloud feedbacks revealed by kernels, and kernel analysis would illuminate the currently ambiguous changes in specific cloud properties contributing to both dynamic- and thermodynamic-induced feedbacks revealed by regime analysis. This paper thus has two primary goals: The first is to demonstrate that these two techniques can be jointly applied to climate model data. We present the mathematical basis for our approach of combining these two analysis techniques in Section 2. The second is to present some novel insights about cloud feedback that come out of doing this diagnostic analysis, which we do in Section 3. With these two goals achieved, we present our conclusions and discuss avenues of future work in Section 4.

## 2 Methodology of Combining Cloud Kernel and Cloud Regime Analyses

At the conceptual level, our analysis is fairly straightforward: We modify the existing cloud regime analysis techniques to operate on joint histograms of cloud-induced radiative anomalies rather than on 2-dimensional cloud radiative effect anomalies. This allows us to derive within- and between-regime changes in cloud-induced radiation anomalies partitioned among the various property changes of interest. A primary technical challenge is that the cloud radiative kernels are defined at monthly resolution, whereas cloud regimes are

101 determined at the daily timescale, so we must assign locations to cloud regimes  
 102 at the daily scale, average them to monthly, and pair them with cloud radiative kernels  
 103 corresponding to each month and regime. After that, standard  
 104 cloud feedback analysis using monthly-resolved data can proceed, now with  
 105 the additional dependence on cloud regime. In the remainder of the section,  
 106 we detail these steps.

107 To begin, note that the value of some cloud-related quantity ( $X$ ) for any  
 108 given region can be expressed as a sum over all  $R$  regimes of the average  $X$   
 109 within a regime ( $X_r$ ), scaled by the relative frequency of occurrence of that  
 110 regime ( $f_r$ ):

$$X = \sum_{r=1}^R f_r X_r. \quad (1)$$

111 Regimes are commonly determined via two approaches: One is to aggregate  
 112 data into meteorological regimes characterized by certain features of the  
 113 large-scale circulation, like 500 hPa vertical motion (Bony et al, 1997, 2004),  
 114 horizontal temperature advection (Norris and Iacobellis, 2005), or proximity  
 115 to cyclones (Tselioudis and Rossow, 2006; Bodas-Salcedo et al, 2012, 2014;  
 116 McCoy et al, 2019, 2020). Another is to determine cloud regimes (sometimes  
 117 called weather states) by applying semi-objective clustering algorithms to the  
 118 cloud characteristics themselves, typically joint histograms of cloud fraction  
 119 segregated by cloud top pressure and optical depth (Jakob and Tselioudis,  
 120 2003; Gordon et al, 2005; Gordon and Norris, 2010; Williams and Tselioudis,  
 121 2007; Williams and Webb, 2009; Oreopoulos and Rossow, 2011; Jin et al,  
 122 2017a,b; Tsushima et al, 2013, 2016). In this study we use regimes that are  
 123 defined using the latter approach, described in more detail below.

124 Anomalies in  $X$  with respect to some base state can be expressed as

$$\Delta X = \sum_{r=1}^R (f_r \Delta X_r + \Delta f_r X_r + \Delta f_r \Delta X_r), \quad (2)$$

125 where the terms on the RHS are the components due to changes in the within-  
 126 regime cloud property, changes in the relative frequency of occurrence of each  
 127 regime, and a covariance term. If  $X$  is cloud radiative effect and these anomalies  
 128 are normalized by the global mean temperature change (e.g., between a  
 129 perturbed and control climate model experiment), these terms represent three  
 130 components of the cloud feedback, albeit a biased measure in the presence  
 131 of clear-sky flux changes (Soden et al, 2004, 2008). These terms have been  
 132 diagnosed and investigated in climate models in several studies (Williams and  
 133 Tselioudis, 2007; Williams and Webb, 2009; Tsushima et al, 2016). Here we  
 134 use Atmospheric Model Intercomparison Project simulations in which observed  
 135 sea surface temperatures (SSTs) and sea ice concentrations are prescribed to  
 136 match observations, known as `amip` experiments. For the climate change re-  
 137 sponse, we use similar atmosphere-only experiments, but the prescribed SSTs  
 138 are uniformly increased by 4 K over the ice-free oceans. These perturbed ex-  
 139 periments are known as `amip4K` in CMIP5 (Taylor et al, 2012) and `amip-p4K`

**Table 1** Models used in this study, along with their model description references and digital object identifiers for their data published to the Earth System Grid Federation. The first five models listed are from CMIP5 and the latter are from CMIP6.

| Model           | Reference             | amip                      | amip+4K                   |
|-----------------|-----------------------|---------------------------|---------------------------|
| CNRM-CM5        | Volodire et al (2019) | 10.1594/WDCC/CMIP5.CEC5am | 10.1594/WDCC/CMIP5.CEC5a4 |
| HadGEM2-A       | Collins et al (2011)  | 10.1594/WDCC/CMIP5.MOGAAm | 10.1594/WDCC/CMIP5.MOGAa4 |
| MIROC5          | Watanabe et al (2010) | 10.1594/WDCC/CMIP5.MIM5am | 10.1594/WDCC/CMIP5.MIM5a4 |
| MPI-ESM-LR      | Stevens et al (2013)  | 10.1594/WDCC/CMIP5.MXELam | 10.1594/WDCC/CMIP5.MXELa4 |
| MRI-CGCM3       | Yukimoto et al (2012) | 10.1594/WDCC/CMIP5.MRMCam | 10.1594/WDCC/CMIP5.MRMCa4 |
| CanESM5         | Swart et al (2019)    | 10.22033/ESGF/CMIP6.3535  | 10.22033/ESGF/CMIP6.3548  |
| CNRM-CM6-1      | Volodire et al (2019) | 10.22033/ESGF/CMIP6.3922  | 10.22033/ESGF/CMIP6.3938  |
| HadGEM3-GC31-LL | Williams et al (2018) | 10.22033/ESGF/CMIP6.5853  | 10.22033/ESGF/CMIP6.5873  |
| IPSL-CM6A-LR    | Boucher et al (2020)  | 10.22033/ESGF/CMIP6.5113  | 10.22033/ESGF/CMIP6.5126  |
| MRI-ESM2-0      | Yukimoto et al (2019) | 10.22033/ESGF/CMIP6.6758  | 10.22033/ESGF/CMIP6.6771  |

140 in CMIP6 (Eyring et al, 2016). We will hereafter refer to these perturbed  
 141 experiments as **amip+4K**.

142 For each model and for the **amip** and **amip+4K** experiments, we use daily-  
 143 resolution surface air temperature, surface upwelling and downwelling clear-  
 144 sky SW fluxes, and the following fields that are produced by the ISCCP sim-  
 145 ulator (Klein and Jakob, 1999; Webb et al, 2001): cloud fractions reported  
 146 in joint cloud top pressure / visible optical depth histograms ( $C$ ), along with  
 147 grid-box mean cloud albedo ( $\alpha$ ), cloud top pressure (CTP), and total cloud  
 148 cover (TCC). The latter three fields are computed ignoring clouds with optical  
 149 depths less than 0.3, the minimum detection threshold of ISCCP. Necessary  
 150 model diagnostics from both **amip** and **amip+4K** experiments are available from  
 151 five CMIP5 models and five CMIP6 models (Table 1).

152 For the reasons discussed in Williams and Webb (2009), we assign each  
 153 daily GCM grid point to a specific cloud regime by finding the minimum  
 154 Euclidean distance between the models' [ $\alpha$  CTP, TCC] vector at that grid  
 155 point and that of the observed centroids. The observed regimes to which we  
 156 assign model data are the eight global weather states derived from ISCCP-  
 157 H observations (Tselioudis et al, 2021). The mean values of the three cloud  
 158 properties for each centroid are given in Table 2 of Tselioudis et al (2021),  
 159 except cloud optical depth rather than albedo is reported. We convert centroid-  
 160 mean optical depth to albedo using the analytic formula:

$$\alpha = \tau^{0.895} / (\tau^{0.895} + 6.82), \quad (3)$$

161 which approximates the ISCCP lookup tables relating grid-mean albedo to  
 162 grid-mean cloud optical thickness (Table 3.1.2 of Rossow et al, 1996), and is  
 163 used by the ISCCP simulator to compute grid-box mean cloud albedo.

164 Before computing Euclidean distances, we normalize the  $\alpha$ , CTP, and TCC  
 165 values by their respective standard deviations, following Jin et al (2017a).  
 166 The standard deviation is calculated across a concatenated vector of all grid  
 167 points and all days over the period 2003-2005 in the **amip** experiment of each  
 168 model. This normalization is necessary because the three fields have different  
 169 units, and is done to both the modeled and observed fields to ensure that the

observational centroids are properly projected into model space. The process of regime assignment yields a binary occurrence matrix ( $n$ ) that is a function of regime ( $r$ ), day ( $d$ ), latitude ( $\phi$ ), and longitude ( $\theta$ ) containing ones where that location belongs to a given regime and zeros where it does not.

Cloud radiative kernels are a function of month, CTP,  $\tau$ , latitude, and – in the case of the SW kernel – clear-sky surface albedo ( $\alpha_{clr}$ ). In order to compute feedbacks we need to aggregate the daily data to monthly resolution and map the SW kernel from its native  $\alpha_{clr}$  space to longitude. For each regime and latitude, we determine the appropriate SW kernel based on the mean clear-sky surface albedo for that regime and latitude. First we compute monthly-averaged climatologies of the data segregated by regime ( $X_r$ ) as the  $n$ -weighted average of daily data ( $x$ ) over all days ( $d$ ) in each of the 12 calendar months ( $m$ ) over the same 9-year portion of the `amip` and `amip+4K` simulations:

$$X_r(m, \phi, \theta) = \frac{1}{N_r} \sum_{y=2000}^{2008} \sum_{d=1}^{D(m_y)} x(d, \phi, \theta) * n_r(d, \phi, \theta), \quad (4)$$

where  $D(m_y)$  is the total number of days within month  $m$  of year  $y$ , and  $N_r$  is the total number of occurrences of each regime in each month and at each location, computed as:

$$N_r(m, \phi, \theta) = \sum_{y=2000}^{2008} \sum_{d=1}^{D(m_y)} n_r(d, \phi, \theta). \quad (5)$$

The results presented hereafter are not sensitive to the number of years or the choice of years analyzed, but geographically-resolved results are less noisy as more years are included. The above process is performed for the cloud fraction histogram (in which case  $x$  and  $X_r$  additionally have dimensions of CTP and  $\tau$ ) and clear-sky surface albedo ( $\alpha_{clr}$ ). The resultant monthly- and regime-resolved  $\alpha_{clr}$  is then used to determine the appropriate SW cloud radiative kernel. This is the same process as described in Zelinka et al (2012b), except here we transform the kernel from its native latitude- $\alpha_{clr}$  space to latitude-longitude space *for each regime*, based on  $\alpha_{clr}(m, \phi, \theta)$  for each regime. (This step is not needed for the LW kernels since they depend only on latitude and not on  $\alpha_{clr}$ .) Hence for each month and location, each cloud regime has its own SW kernel that is appropriate for the average  $\alpha_{clr}$  present on the days within the month assigned to that regime. Finally, we define the relative frequency of occurrence ( $f_r$ ) as the fraction of days within a month that a regime is present at a given location:

$$f_r(m, \phi, \theta) = \frac{N_r(m, \phi, \theta)}{\sum_{r=1}^R N_r(m, \phi, \theta)}. \quad (6)$$

The sum of  $f_r$  over all regimes equals 1 for that location. Hererafter we drop the notation specifying that regime-segregated quantities are additionally functions of month, latitude, and longitude.

This analysis yields climatological cloud fraction histograms ( $C_r$ ), cloud radiative kernel histograms ( $K_r$ ), and relative frequency of occurrences ( $f_r$ ) that are segregated into 8 cloud regimes at each latitude and month, for both the **amip** and **amip+4K** experiments. Replacing  $X_r$  with the product of  $C_r$  and  $K_r$  in Equation (2), we can now express the cloud feedback as:

$$\lambda_{cld} = \frac{1}{\Delta T_s} \sum_{r=1}^R K_r (f_r \Delta C_r + \Delta f_r C_r + \Delta f_r \Delta C_r), \quad (7)$$

where  $T_s$  is the global mean surface air temperature,  $\Delta$  refers to the difference between **amip+4K** and **amip** climatologies, and any field without a  $\Delta$  preceding it refers to the **amip** climatology.

The key novelty of our analysis is that  $X_r$  in (2) is replaced with  $C_r K_r$  in (7), where  $C_r$  and  $K_r$  are additionally functions of cloud top pressure and visible optical depth, giving us the ability to further break these terms down into components due to individual cloud property changes, something which cannot be done if  $X$  refers to CRE. We will now discuss this break down in greater detail.

The first term on the RHS of Eq 7 ( $f_r \Delta C_r K_r$ ) is the cloud feedback arising from changes in within-regime cloud properties, and the third ( $\Delta f_r \Delta C_r K_r$ ) is the covariance term. Both of these naturally break down into amount, altitude, and optical depth components (Zelinka et al., 2012a, 2013). As shown below the covariance term is generally very small.

The second term on the RHS of Eq 7 ( $\Delta f_r C_r K_r$ ) is the cloud feedback arising from changes in the relative frequency of occurrence of each regime. Because it is simply a scalar multiplied by the cloud fraction histogram, it can only cause an increase or decrease in the total cloud amount but not a change to the CTP or  $\tau$  distribution. Hence this can only bring about a cloud amount feedback, while the altitude and optical depth feedbacks are by definition zero. However, it is desirable to quantify cloud property feedbacks due to changes in the frequency of occurrence of regimes with different properties. For example, we would like to quantify the optical depth feedback arising from shifts from thinner-than-average to thicker-than-average regimes, which would be embedded in this second term. To do so, we express this term as the sum of four components:

$$\Delta f_r C_r K_r = \Delta f_r (\bar{C} \bar{K} + \bar{C} K'_r + C'_r \bar{K} + C'_r K'_r), \quad (8)$$

where  $\bar{C}$  is the annual- and regime-averaged histogram at each location, and  $C'_r = C - \bar{C}$  contains all monthly- and regime-dependent deviations of the histogram from this.  $K'_r$  and  $\bar{K}$  are defined in the same manner. Of these terms, the third ( $\Delta f_r C'_r \bar{K}$ ) turns out to be dominant when results are summed over all regimes. This makes sense because regimes defined by clustering cloud fraction histograms essentially guarantees that across-regime variations in climatological cloud fraction histograms are substantial. These variations are much larger than across-regime variations in kernels (term 2) or their covariances (term 4). Moreover, since the across-regime sum of  $\Delta f_r$  is zero by definition,

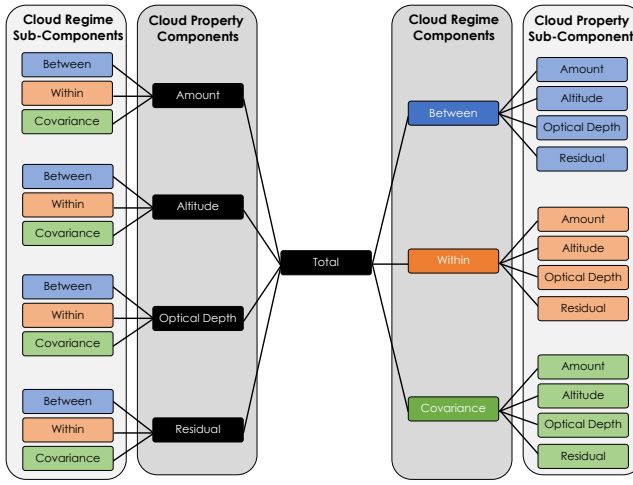


**Fig. 1** Schematic of the cloud feedback decomposition. We decompose the total cloud feedback into cloud regime components (within-regime, between-regime, and covariance terms), which are further broken down into cloud property sub-components (amount, altitude, optical depth, and residual terms). These resulting cloud property sub-components are reorganized on the left branch of the diagram such that each cloud regime sub-component is grouped by cloud property component. Feedback sub-components on the left- and right-most branches with the same colors are identical, but simply organized differently to aid complementary interpretations.

244 the across-regime sum of a scalar ( $\bar{K}$ ) times  $\Delta f_r$  (term 1) must also be zero.  
 245 Therefore, we can express Equation 8 as:

$$\Delta f_r C_r K_r = \Delta f_r C'_r \bar{K} + \epsilon, \quad (9)$$

246 which leads to our ultimate expression for the cloud feedback breakdown:

$$\lambda_{clu} = \frac{1}{\Delta T_s} \sum_{r=1}^R (\Delta f_r C'_r \bar{K} + f_r \Delta C_r K_r + \Delta f_r \Delta C_r K_r + \epsilon). \quad (10)$$

247 We shall hereafter refer to these first three components as the “between-  
 248 regime”, “within-regime”, and “covariance” components. As will be shown be-  
 249 low, the neglected “between-regime” components encapsulated in  $\epsilon$  are small.  
 250 A schematic illustrating the complete break-down of cloud feedback produced  
 251 in this study is shown in Figure 1.

252 The analysis is performed for LW, SW, and net (LW+SW) cloud feed-  
 253 backs, but for the sake of simplifying the presentation of results, we will focus  
 254 hereafter on just the SW cloud feedback.

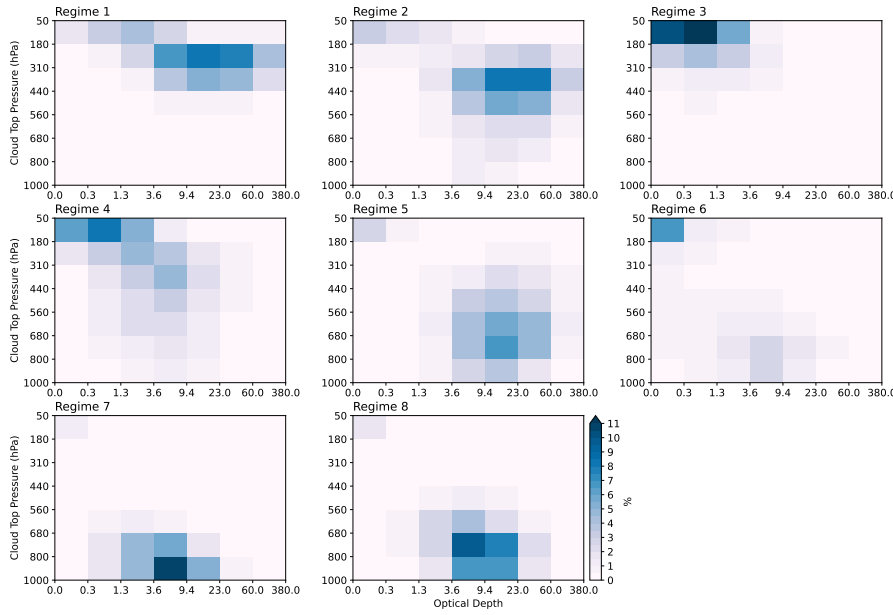


**Fig. 2** Cloud fraction histograms for each regime, averaged across models and globally.

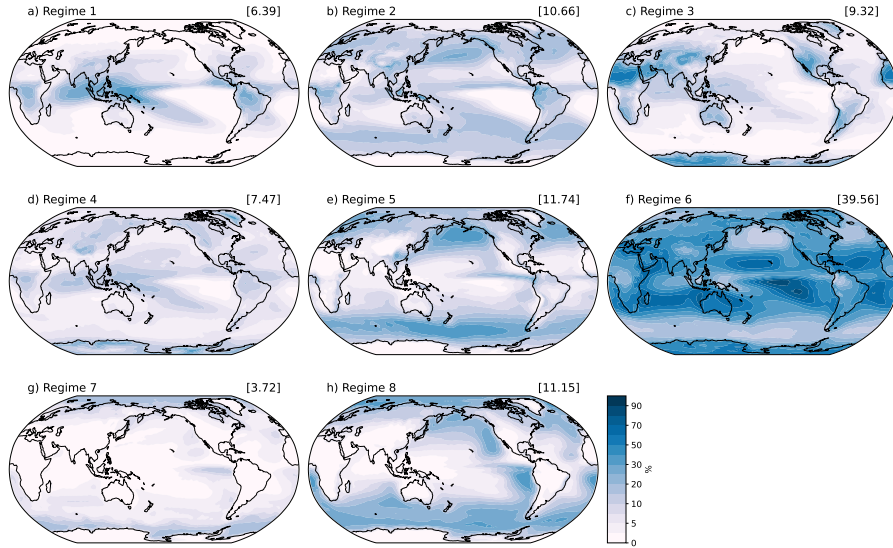


**Fig. 3** Relative frequency of occurrence of each regime, expressed as a percentage of time that a given regime is present at each grid point, averaged across models. The global average RFO is displayed in the title of each panel.

---

**255 3 Results****256 3.1 Cloud Regime Characteristics**

257 Multi-model mean cloud fraction histograms averaged within each of the cloud  
258 regimes and maps showing the relative frequency of occurrence of each cloud  
259 regime are shown in Figures 2 and 3, respectively. Global-mean values of total  
260 cloud cover, albedo, cloud top pressure, and relative frequency of occurrence  
261 for each regime averaged across all models (and their across-model standard  
262 deviation) are provided in Table 2. Comparing these figures with their obser-  
263 vational counterparts shown in Figure 1 of Tselioudis et al (2021), we see many  
264 qualitative similarities, as expected given that we are matching modeled cloud  
265 properties to the observed centroids, as well as some noteworthy differences.  
266 Regime 1 contains primarily high, thick clouds and is prevalent in regions of  
267 tropical deep convection, similar to observations. Regime 2 contains moder-  
268 ately thick high clouds (as well as some lower clouds) that are prevalent in the  
269 middle-latitude storm-track region. Unlike in the observations, this regime is  
270 not confined to middle latitudes and also occurs frequently in tropical ascent  
271 regions in the models. Regime 3 is a cirrus cloud category, with very high thin  
272 clouds that are prevalent in the Indo-Pacific warm pool region, but also over  
273 subtropical land regions, similar to observations. Regime 4 contains a broad  
274 range of cloud top pressures and optical thicknesses but is dominated by high,  
275 thin clouds, similar to the observations. Unlike in observations, however, this  
276 regime occurs frequently outside of the polar regions, including in tropical  
277 ascent regions. Optically thick mid-level clouds that are prevalent over the  
278 middle latitude oceans characterize Regime 5, in qualitative agreement with  
279 the observations. Unlike the observations, the regime occurs often in the East  
280 Pacific ITCZ region, and the overall frequency of occurrence is roughly twice  
281 as large as in observations. As in observations, Regime 6 is the most frequently  
282 observed regime (RFO of nearly 40%), and contains a mix of scattered thin  
283 cumulus and cirrus clouds, with generally small cloud fractions. It is most  
284 prevalent over trade cumulus regions. Regimes 7 and 8 are dominated by low  
285 clouds that are prevalent over cold sea surface temperatures, as in observa-  
286 tions. Regime 7 contains lower-topped, slightly thinner clouds with smaller  
287 fractional coverage than Regime 8, which led Tselioudis et al (2021) to classify  
288 these as shallow cumulus and stratocumulus clouds, respectively. Unlike in  
289 observations where these two regimes occur with similar frequency, the RFO  
290 of Regime 8 is three times greater than that of Regime 7 in the model mean.

291 Some of the model-observation discrepancies mentioned above may be alle-  
292 viated by performing the minimum Euclidean distance calculation with the full  
293 information content of the histograms (Williams and Tselioudis, 2007) rather  
294 than the simplified 3-element vector (Williams and Webb, 2009), though we  
295 have not tested this. However, this paper is not concerned with evaluating  
296 models' ability to simulate the correct within-regime cloud characteristics or  
297 the correct frequency of occurrence of the various regimes. Such model eval-  
298 uation studies have already been done previously, including for the regimes

**Table 2** Multi-model mean global mean total cloud cover (TCC), cloud albedo ( $\alpha$ ), cloud top pressure (CTP), and relative frequency of occurrence (RFO) in the control climate. The  $1-\sigma$  range across models is shown in parenthesis.

| Regime | TCC [%]    | $\alpha$ [%] | CTP [hPa]    | RFO [%]    |
|--------|------------|--------------|--------------|------------|
| 1      | 83.8 (9.7) | 54.7 (2.7)   | 281.7 (14.6) | 6.4 (1.6)  |
| 2      | 80.9 (4.5) | 57.8 (3.6)   | 429.9 (6.2)  | 10.7 (3.2) |
| 3      | 42.7 (8.5) | 18.8 (2.0)   | 239.4 (23.6) | 9.3 (3.7)  |
| 4      | 68.4 (6.6) | 32.2 (1.7)   | 369.3 (17.8) | 7.5 (2.5)  |
| 5      | 75.4 (5.5) | 57.9 (3.3)   | 615.3 (15.5) | 11.7 (4.1) |
| 6      | 26.5 (4.0) | 37.4 (4.7)   | 648.5 (41.4) | 39.6 (7.0) |
| 7      | 61.6 (4.9) | 39.2 (3.8)   | 805.2 (25.2) | 3.7 (1.6)  |
| 8      | 71.1 (6.0) | 48.6 (3.9)   | 723.5 (26.1) | 11.1 (3.2) |

**Table 3** As in Table 2, but showing the response to +4K warming for each regime.

| Regime | $\Delta TCC$ [%/K] | $\Delta \alpha$ [%/K] | $\Delta CTP$ [hPa/K] | $\Delta RFO$ [%/K] |
|--------|--------------------|-----------------------|----------------------|--------------------|
| 1      | -0.28 (0.47)       | 0.24 (0.17)           | -3.06 (0.94)         | 0.37 (0.24)        |
| 2      | -0.70 (0.36)       | 0.27 (0.15)           | -0.47 (0.53)         | 0.03 (0.10)        |
| 3      | -0.08 (0.23)       | 0.18 (0.09)           | -3.23 (1.17)         | 0.17 (0.21)        |
| 4      | -0.51 (0.27)       | 0.15 (0.07)           | -3.4 (1.16)          | -0.18 (0.11)       |
| 5      | -0.62 (0.16)       | 0.29 (0.10)           | 0.68 (0.98)          | 0.07 (0.22)        |
| 6      | -0.28 (0.21)       | 0.36 (0.11)           | -0.88 (1.21)         | 0.11 (0.36)        |
| 7      | -0.28 (0.15)       | 0.16 (0.06)           | -0.14 (0.65)         | -0.24 (0.18)       |
| 8      | -0.49 (0.19)       | 0.18 (0.10)           | -0.00 (0.70)         | -0.32 (0.21)       |

used in this study (Tselioudis et al, 2021). Our objective, rather, is to demonstrate the utility of employing a regime framework to better understand the processes driving cloud feedbacks, allowing us to distinguish within- from between-regime cloud changes in contributing to the various cloud property feedbacks, and vice versa. Such an analysis does not require that models' cloud regime properties match observations particularly well, only that their clouds can be grouped into a set of regimes with reasonably-distinct and physically-interpretable characteristics that facilitates such a breakdown. The attribution of between-regime changes to large-scale atmospheric dynamics is supported by the fact that the cloud regimes show skill in tracing distinct meteorological states and cloud formation mechanisms, as demonstrated in Tselioudis et al (2021). As will be demonstrated below, our breakdown is not sensitive to the exact definition of regimes. Hence the results are resilient to reasonable variations in how exactly the regimes are initially defined.

### 3.2 Changes in Regime-Averaged Properties

To aid in interpreting the feedback results shown below, in Figure 4 we show the change in the regime-averaged cloud fraction histograms under +4K warming, averaged across the 10 models analyzed (Table 1). Table 3 shows changes in globally-averaged cloud properties in each regime, averaged across models. In all regimes, the cloud fraction decreases for mid-level clouds of most thicknesses and for clouds with highest CTPs (i.e., nearest to the surface). The

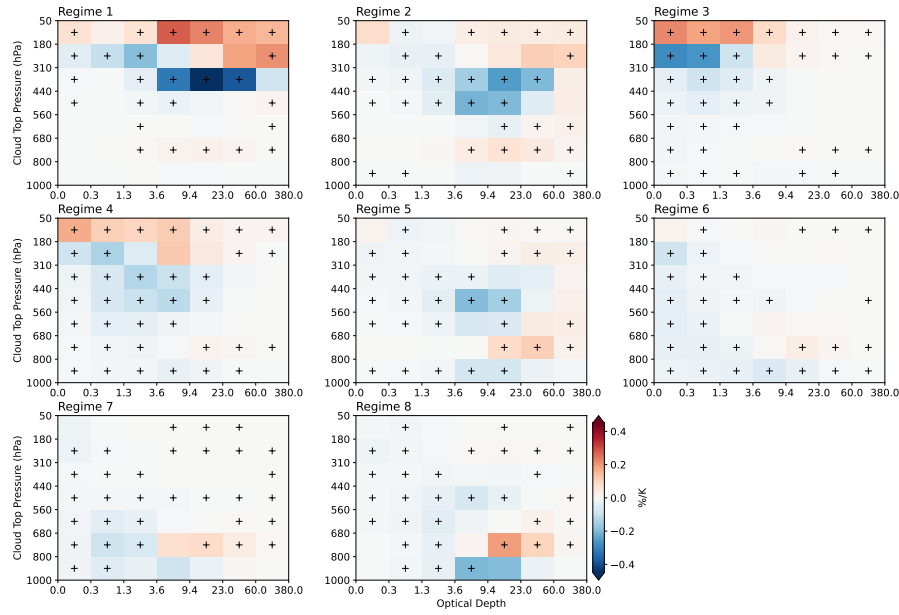


**Fig. 4** Temperature-mediated change in cloud fraction histograms for each regime, averaged across models and globally. Stippling indicates locations where at least 8 out of 10 models agree on the sign of the change.

fraction of clouds at the highest altitudes increases, most notably in regimes dominated by high clouds (Figure 4, Regimes 1-4). This, coupled with the strong decreases in cloud fractions at levels immediately below, indicates an upward shift of cloud tops. This upward shift has a theoretical basis, is simulated in high resolution models, and has been observed in response to climate variability and secular trends (Sherwood et al (2020) and references therein). Increases are also apparent for clouds with CTPs between 680 and 800 hPa in most regimes, but most prominently in the cumulus and stratocumulus regimes (Figure 4, Regimes 7 and 8). In all regimes, these increases occur immediately above bins with similar decreases, again suggesting an upward shift of the low-level cloud population with warming.

Aside from the aforementioned changes in cloud top altitude, two other gross cloud properties exhibit systematic changes with warming: In every regime, total cloud fraction decreases and optical depth increases. The former is difficult to discern directly from the histograms, but is indicated by the change in total cloud fraction shown in Table 2. The latter can be inferred from the overall tendency for an increase in cloud fraction in higher optical depth bins of the histograms along with corresponding decreases in cloud fraction in the thinner bins, and verified in the  $\Delta\alpha$  column of Table 3. Hence, for clouds of a given regime, warming causes them to systematically rise, increase in albedo, and decrease in coverage. As will be seen below, this leads

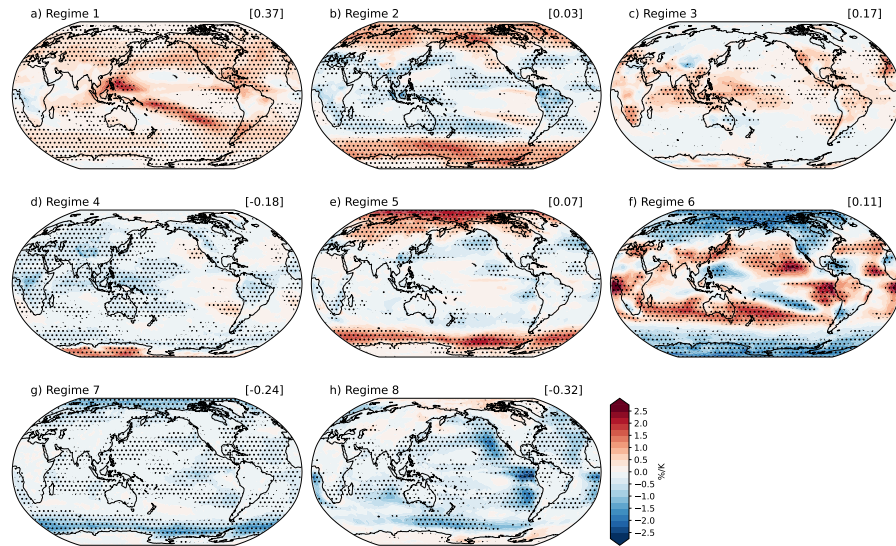


**Fig. 5** Temperature-mediated change in the relative frequency of occurrence of each regime, averaged across models. The global average RFO change is displayed in the title of each panel. Stippling indicates locations where at least 8 out of 10 models agree on the sign of the change.

341 to within-regime cloud feedback components that are highly consistent across  
342 models and across regimes.

343 The change in regime relative frequency of occurrence maps is shown in  
344 Figure 5, and in Figure 6 we show the zonal-mean RFO and its change. The  
345 RFO of high cloud regimes 1 and 3 increase systematically, most prominently  
346 where these regimes are prevalent climatologically. Regimes 4, 7, and 8 all  
347 show large decreases in RFO at nearly all latitudes, with the latter being  
348 especially prominent in the eastern ocean basins. These decreases in the RFO  
349 of Regimes 7-8 coincide with prominent increases in the RFO of Regime 6,  
350 highly suggestive of a stratocumulus-to-cumulus transition.

351 Comparing Figures 3 and 5, and panels (a) and (b) of Figure 6, one can dis-  
352cern poleward shifts of cloud types. This is apparent for Regimes 2 and 5, for  
353 which increases in RFO occur at latitudes just poleward of the control-climate  
354 RFO maximum, where RFO is strongly decreasing with latitude. The opposite  
355 response is also apparent at locations just equatorward of the control-climate  
356 RFO maximum. Both of these regimes correspond to storm-track clouds, which  
357 are expected to shift poleward with warming (Yin, 2005; Barnes and Polvani,  
358 2013). Similarly, increases in the RFO of Regime 6 peak near 40S and 40N,  
359 where its control-climate RFO falls off rapidly with latitude. This is sugges-  
360tive of a poleward expansion of the subtropics and of the already-ubiquitous  
361 cumulus regime.

362 Overall, the cloud population tends to shift from cloudier and thicker  
363 regimes (2, 5, and 8) towards less-cloudy and thinner regimes (3 and 6) at

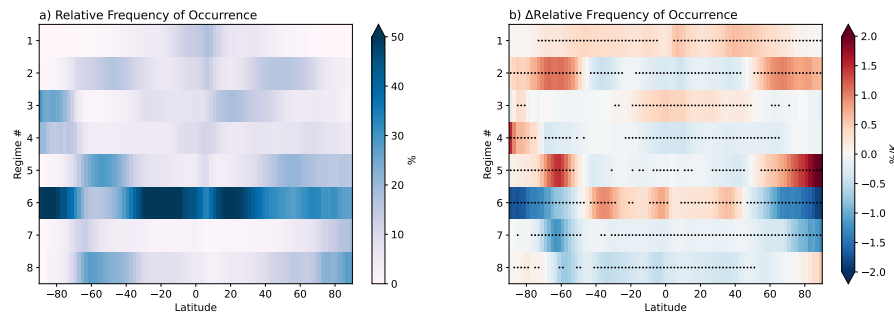


**Fig. 6** (a) Zonally averaged relative frequency of occurrence of each cloud regime, averaged across models, and (b) its temperature-mediated change in response to +4K warming. Stippling in (b) indicates locations where at least 8 out of 10 models agree on the sign of the change.

364 low latitudes, with the opposite response in the extratropics. Put another  
 365 way, the regimes characterized by bright and extensive clouds shift poleward  
 366 with warming, and in their wake the conditions are favorable for regimes char-  
 367 acterized by thinner and less extensive clouds.

### 368 3.3 Global mean feedback decomposition

369 As mentioned above, the cloud feedback has previously been broken down  
 370 into within-regime, between-regime, and covariance terms (Williams and Tse-  
 371 lioudis, 2007; Williams and Webb, 2009; Tsushima et al, 2016), but these have  
 372 not been further segregated into their amount, altitude, and optical depth  
 373 sub-components. Likewise, the previously-diagnosed amount, altitude, and op-  
 374 tical depth feedback components (Zelinka et al, 2012b, 2013, 2016) have not  
 375 been further broken down into their within, between, and covariance sub-  
 376 components. In Figure 7 we perform this more extensive breakdown for the  
 377 global-mean SW cloud feedback.

378 At the center of the figure is the true global mean SW cloud feedback com-  
 379 puted without performing any breakdown, labeled as “No Breakdown”. The  
 380 four columns to the left (a-d) provide the cloud property breakdown of this  
 381 feedback, which are further broken down into cloud regime sub-components  
 382 and their sum. The four columns to the right (e-h) provide the same informa-  
 383 tion, but organized differently: the cloud regime breakdown of the feedback,  
 384 further broken down into cloud property sub-components and their sum. (The  
 385 kernel residual term is not shown because it is very small in all cases.)

386 Consider first Figure 7e, which shows the sum of all terms in Equation 10  
 387 except the  $\epsilon$  term. That the first sub-column within this category (“Total”)  
 388 closely matches the “No Breakdown” results indicates that the neglected  $\epsilon$   
 389 terms are small and that we can successfully interpret the between-regime  
 390 component as primarily being due to  $\Delta f_r C'_r \bar{K}$  in Equation 8. This also allows  
 391 us to break this between-regime component into amount, altitude, and optical

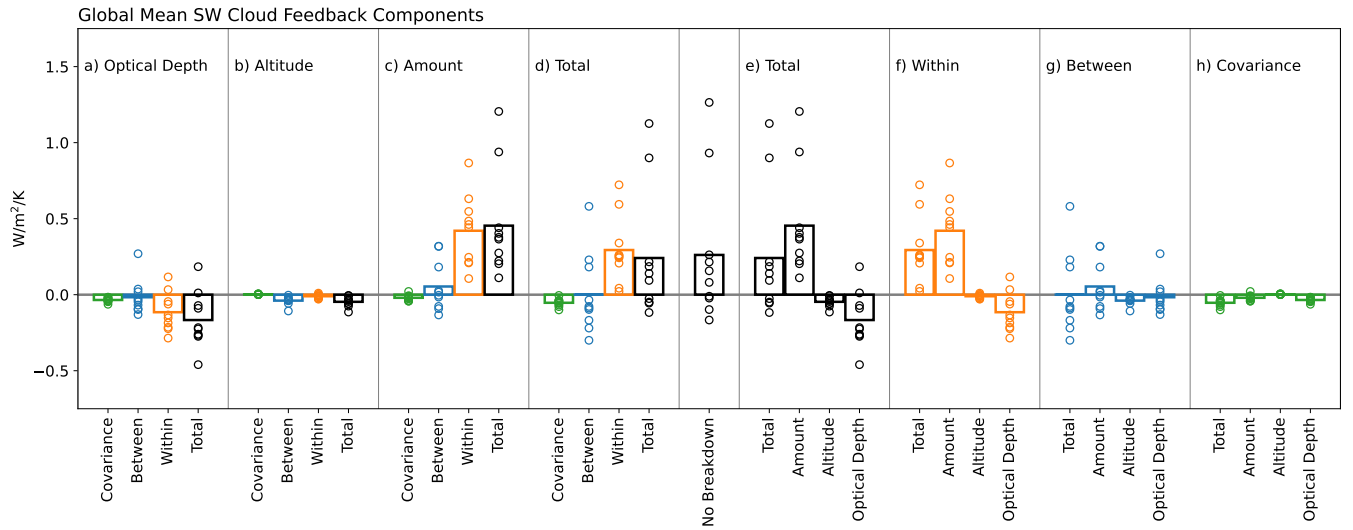


**Fig. 7** Globally averaged SW cloud feedbacks for each model, broken down into cloud property and cloud regime components. The “No Breakdown” cloud feedback, which is computed without performing any regime decomposition, serves as a ground-truth for the sum of components that are shown to the left and right. Results are identical to the left and right of the center column, but organized differently to facilitate complementary comparisons. Columns (a)-(d) show cloud property components along with the cloud regime sub-components comprising them, while columns (e) - (h) show cloud regime components along with the cloud property sub-components comprising them.

392 depth terms, which are shown in Figure 7g and discussed below. The global  
 393 mean SW cloud amount component is robustly positive across the 10 models  
 394 analyzed, while the altitude component is unsurprisingly small with little inter-  
 395 model spread. The optical depth component is negative in all but two models,  
 396 with a multi-model average that is smaller in magnitude than that of the  
 397 amount component, leading to the overall positive multi-model mean SW cloud  
 398 feedback.

399 The within-regime component (Figure 7f) is robustly positive across mod-  
 400 els, and is made up of two robust feedbacks of opposite sign: a robustly positive  
 401 amount component and a smaller optical depth component that is negative  
 402 in all but two models. The within-regime component of the total cloud feed-  
 403 back, as well as its cloud property sub-components, are remarkably similar  
 404 to those of the total cloud feedback (compare panels e and f). This is espe-  
 405 cially true for the multi-model mean results, whereas the inter-model spread  
 406 of the within-regime components are reduced relative to the full feedback.  
 407 Hence, for the multi-model mean, one can largely attribute the total overall  
 408 SW cloud feedback and its cloud property sub-components to within-regime  
 409 cloud changes. This may indicate that – once obfuscating effects of changes  
 410 in large-scale dynamics are removed – the temperature-mediated response of  
 411 clouds is very systematic across models. That is, within distinct cloud regimes

412 or weather states, warming causes a systematic decrease in the fractional cov-  
413 erage of clouds – a positive amount feedback – and a systematic increase in  
414 the albedo of clouds – a negative optical depth feedback. Below we will fur-  
415 ther show that this uniformity in sign of the within-regime amount and optical  
416 depth components holds not just across models in the global mean sense, but  
417 also geographically and across regimes.

418 In contrast to the within-regime component, the between-regime compo-  
419 nent exhibits substantial spread across models but with a multi-model mean  
420 value that is very close to zero (Figure 7g, ‘Total’ sub-column). Similarly, the  
421 cloud property sub-components of the between-regime feedback exhibit sub-  
422 stantial inter-model variations that straddle zero, leading to near-zero contribu-  
423 tions to the multi-model average total cloud feedback. This indicates that,  
424 averaged over the entire planet, shifts among cloud types (likely caused by  
425 changes in large-scale meteorology) can cause large feedbacks of either sign in  
426 models, but averaged across all models, these shifts make essentially no con-  
427 tribution to the global, ensemble mean feedback. However, as will be shown  
428 below, the between-regime component can be very important locally, where  
429 shifts among cloud regimes with different properties cause substantial radiative  
430 impacts, often of larger magnitude than the within-regime component. These  
431 local contributions can either reinforce or counteract the local within-regime  
432 contributions.

433 The global mean covariance terms (Figure 7h) are very small, as expected,  
434 and will not be discussed further.

435 Turning to the left four columns of Figure 7, we see the same information,  
436 but re-organized so as to better illuminate how within- and between-regime  
437 changes contribute to each of the cloud property feedback components – in-  
438 formation that was not revealed in previous studies performing this decompo-  
439 sition (e.g., Zelinka et al (2012a, 2013, 2016)).

440 From Figure 7d, it is clear that the total cloud feedback, on average across  
441 models, is entirely coming from the systematically positive within-regime com-  
442 ponent. The between-regime component, in contrast, can be large and of either  
443 sign in models, but averages to a near-zero value across models. The SW cloud  
444 amount feedback is robustly positive in all models, with a large multi-model  
445 mean (Figure 7c). Again, this comes almost entirely from the within-regime  
446 component, which is systematically positive in all models but with inter-model  
447 spread that is smaller than the total amount component. The between-regime  
448 cloud amount feedback varies widely among models but is close to zero on av-  
449 erage across models. Owing to the weak dependence of reflected SW radiation  
450 on cloud top pressure, the SW altitude feedback and all of its sub-components  
451 are very small (Figure 7b). As previously mentioned, the optical depth feed-  
452 back is negative in all but two models and is moderately negative on average  
453 across models (Figure 7a, ‘Total’ sub-column). The multi-model mean value  
454 comes solely from the within-regime component, whereas the between-regime  
455 component straddles zero.

456 From these global mean results, we conclude that, for any given model,  
457 both the within-regime and between-regime components can be substantial.

458 However, their roles in the multi-model mean feedback are rather different: The  
459 between-regime components tend to exhibit substantial inter-model spread  
460 that straddles zero, leading to a multi-model contribution that is negligible.  
461 In contrast, the within-regime components tend to be of uniform sign across  
462 models (systematically positive for cloud amount and nearly systematically  
463 negative for cloud optical depth), such that they are the primary contributor  
464 to the positive ensemble-mean SW cloud feedback. Hence a robust signal of  
465 temperature-mediated cloud behavior across models becomes apparent when  
466 controlling for changes in large-scale meteorology, and one can attribute the  
467 positive multi-model mean SW cloud feedback to a robustly positive within-  
468 regime SW cloud amount feedback that is partially counteracted by a nearly  
469 robustly negative within-regime SW cloud optical depth feedback.

470 Because the covariance and altitude components have been shown here  
471 to be small, we will focus hereafter on the amount and optical depth cloud  
472 property components and on the within- and between-regime components so  
473 as to simplify the number of fields to consider.

#### 474 3.4 Spatial structure of the multi-model mean SW cloud feedback and its 475 components

476 The complementary views of the multi-model mean cloud feedback provided by  
477 the marriage of regime-based and kernel-based decompositions are exemplified  
478 in Figure 8. The total SW cloud feedback (a) is broken down in column 1 into  
479 its amount (d) and optical depth (g) components, and in row 1 into its between-  
480 regime (b) and within-regime (c) components. Note that the global mean value  
481 shown in (a) equals the sum of global mean values shown in (b) and (c), plus  
482 the covariance term which is not shown. It also equals the sum of global mean  
483 values shown in (d) and (g), plus the altitude and kernel residual terms which  
484 are not shown because they are negligibly small. The between- and within-  
485 regime components are broken down into their amount and optical depth sub-  
486 components in columns 2 and 3, respectively. Equivalently, the amount and  
487 optical depth components are broken down into their between- and within-  
488 regime sub-components in rows 2 and 3, respectively.

489 SW cloud feedback is positive nearly everywhere equatorward of about 50  
490 degrees latitude and negative elsewhere, with large negative values centered  
491 around 60 degrees in both hemispheres (Figure 8a). Large positive feedbacks  
492 are present throughout the subtropical oceans and tropical land regions. This  
493 overall pattern emerges due to the superposition of a strong positive amount  
494 feedback (Figure 8d) at low latitudes with maxima in the subtropics that falls  
495 to near-zero or weak negative values poleward of about 50 degrees latitude,  
496 and a strong negative optical depth feedback (Figure 8g) in the extratropics  
497 that peaks around 60 degrees and that falls off or becomes weakly positive  
498 equatorward of about 40 degrees latitude. Alternatively, one can describe the  
499 mean SW cloud feedback pattern as the superposition of a very spatially het-  
500 erogeneous between-regime component (Figure 8b) that closely matches the

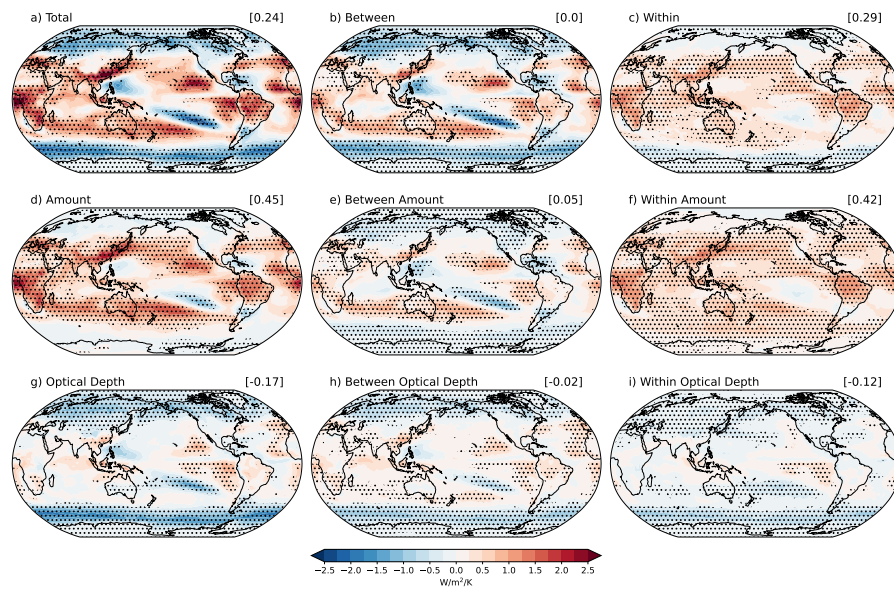


**Fig. 8** (a) Multi-model mean total SW cloud feedback and its breakdown into the dominant terms comprising it: (b) and (c) show the between-regime and within-regime components, while (d) and (g) show the amount and optical depth components. The amount component (d) is broken down into its between-regime and within-regime sub-components in (e) and (f), respectively. The optical depth component (g) is broken down into its between-regime and within-regime sub-components in (h) and (i), respectively. Stippling indicates locations where at least 8 out of 10 models agree on the sign of the change.

overall SW cloud feedback pattern, and a much more spatially homogeneous within-regime component (Figure 8c) that is positive everywhere except at high latitudes.

As summarized in Sherwood et al (2020), the positive low-latitude SW cloud amount feedbacks are consistent with a large body of work concluding that cloud cover should decrease with warming, including for tropical high clouds (Zelinka and Hartmann, 2011; Bony et al, 2016), tropical marine low clouds (Myers and Norris, 2016; Klein et al, 2017), and low clouds over land (Del Genio and Wolf, 2000; Zhang and Klein, 2013). Likewise, the latitudinally-varying response of cloud optical depth to warming is consistent with previous modeling studies, though observational analyses suggest a weaker negative extratropical feedback than produced in most models (Tselioudis et al, 1992; Eitzen et al, 2011; Gordon and Klein, 2014; Terai et al, 2016; Myers et al, 2021).

The tendency for the SW cloud amount component (Figure 8d) to be positive at low latitudes and small or negative at high latitudes is primarily established by the between-regime component (Figure 8e), which shares this overall pattern. This means that, generally speaking, shifts from regimes with large cloud fraction to small cloud fraction occur at lower latitudes, particularly in the subtropics, and shifts from regimes with small cloud fraction to large cloud

fraction occur at higher latitudes, with the overall radiative impact of these cloud amount changes being strongly muted ( $0.05 \text{ W/m}^2/\text{K}$  on average; Figure 8e). In contrast, the within-regime cloud amount feedback (Figure 8f) is nearly uniformly positive across the globe, with substantial model agreement on the sign of the response (as indicated by the ubiquitous stippling). This indicates that, once controlling for population shifts among regimes, the temperature mediated response of nearly all clouds globally is to decrease in areal coverage. This leads to a strong positive amount component from within-regime cloud property changes that is roughly equal to the full amount feedback. We will show below that this feedback component is uniformly positive even at the individual cloud regime level, not just when summing across cloud regimes. The local maxima in the amount feedback in the subtropics are regions where both the between- and within-components are positive. In these regions, both shifts towards regimes with smaller cloud fraction as well as decreases in cloud fraction within the regimes that are present reinforce one another. In contrast, the weak overall cloud amount feedback in the extratropics (Figure 8d) arises because the negative contribution from shifts toward regimes with extensive cloud cover at the expense of regimes with less extensive cloud cover (Figure 8e) counteracts the positive contribution from decreases in cloud fraction within the regimes that are present (Figure 8f). Elucidation of which regimes are favored and disfavored with warming were discussed in Section 3.2 (Figures 5 and 6) and their individual radiative contributions are discussed further below.

Consider now the SW cloud optical depth feedback and its sub-components (row 3). In a similar way to the amount component, the between-regime optical depth sub-component (Figure 8h) is small in the global mean but largely establishes the overall spatial structure of the optical depth feedback (Figure 8g), while the within-regime sub-component (Figure 8i) is much more uniformly negative and the dominant contributor to the global mean feedback. An exception is the Eastern Pacific stratocumulus regions, which exhibit robustly positive within-regime contributions to the optical depth feedback (Figure 8i). Shifts from regimes with small optical depth to regimes with large optical depth occur at high latitudes, and these coincide with regions where the optical depth of clouds increases within the regimes already present, resulting in the very strong negative extratropical optical depth feedback (Figure 8g-i). This is especially prominent over the Southern Ocean and the high northern hemisphere continents. In contrast, throughout much of the low-to-middle latitudes, the within- and between-regime sub-components oppose each other, resulting in weak overall optical depth feedback. For example in the North and South Pacific and southern Indian Oceans, shifts from thicker to thinner regimes make weak positive contributions to the optical depth feedback, but this is counteracted by the thickening of the clouds within regimes that are already present (Figure 8g-i).

Returning to a question posed in the introduction, it is now clear that the negative SW cloud optical depth feedback over the Southern Ocean (40–70S) receives contributions from both increased frequency of occurrence of

567 thicker cloud types relative to thinner cloud types, as well as increases in the  
568 albedo of clouds of a given morphology. Given that both components matter,  
569 we cannot focus solely on constraining changes in meteorology that determine  
570 cloud morphology or solely on constraining thermodynamic processes that  
571 affect cloud reflectivity within a given meteorological condition.

572 Let us briefly discuss the contributors to the between-regime and within-  
573 regime SW cloud feedbacks (columns 2 and 3, respectively). The near-zero  
574 global mean between-regime feedback (Figure 8b) results from the super-  
575 position of amount (Figure 8e) and optical depth (Figure 8h) sub-components  
576 that share very similar spatial structures – both are positive at low latitudes  
577 and negative at high latitudes, with nearly coincident zero-crossings at 45  
578 degrees latitude. This is to be expected because the regimes with large cloud  
579 fractions also have large optical depths (Table 2). Therefore, an increase in the  
580 RFO of cloudier/thicker regimes at the expense of less cloudy/thinner regimes  
581 will result in similar negative contributions to the amount and optical depth  
582 feedbacks (e.g., over the high latitudes), and vice versa. In contrast, the within-  
583 regime SW cloud feedback (Figure 8c) results from a near-uniform positive  
584 amount sub-component (Figure 8f) that is partially counteracted at most loc-  
585 ations by a near-uniformly negative optical depth sub-component (Figure 8i).  
586 The latter is large enough at high latitudes to dominate over the amount sub-  
587 component. Though exhibiting less spatial heterogeneity than the between-  
588 regime component, what little heterogeneity exists in the within-regime com-  
589 ponent belies the vast regions of the globe in (Figure 8f) and (Figure 8i) over  
590 which at least 8 out of 10 of the models agree on the sign of the feedback.

591 The results above indicate that much of the spatial structure of cloud feed-  
592 back can be interpreted as due to changes in meteorology, which influences the  
593 relative amounts of the various cloud morphologies present, but which makes  
594 a small globally-averaged radiative impact. Excluding this component and fo-  
595 cusing on the within-regime cloud changes, in contrast, highlights much more  
596 spatially uniform and systematic underlying cloud changes, whose radiative  
597 impact provides the dominant contribution to the globally averaged feedback.

598 To what extent is interpretation of the between- and within-regime feed-  
599 back components complicated by the fact that regimes are defined by the cloud  
600 properties themselves rather than by exogenous fields characterizing relevant  
601 aspects of the meteorological environment (e.g., 500 hPa vertical velocity)?  
602 Consider a case where clouds of a given morphology at a given location thicken  
603 with warming. If this thickening is relatively small, one would expect this to  
604 be classified as a negative within-regime SW optical depth feedback. But if  
605 the thickening were sufficiently large, that location could be re-classified to a  
606 different, thicker cloud regime resulting in a negative *between-regime* SW opti-  
607 cal depth feedback. Fundamentally, the same cloud property change occurred  
608 in both cases, but our analysis would ascribe a different meanings to them,  
609 which is not desired. It is worth recalling, however, that locations are assigned  
610 to regimes based on the combination of 3 cloud properties: albedo, cloud top  
611 pressure, and total cloud fraction, so it is not guaranteed that thickening would  
612 necessarily lead to reclassification to a thicker cloud regime if the cloud top

613 pressure and total cloud fraction remain more similar to the original regime  
614 than to the thicker regime.

615 Nevertheless, if such a scenario were common, one would expect high  
616 pattern correlations between the within- and between-regime cloud feedback  
617 maps. Comparing the spatial patterns of the between-regime and within-  
618 regime feedbacks (Figure 8, columns 2 and 3), it is clear that while there  
619 are some similarities, the patterns are largely distinct. Uncentered pattern  
620 correlations between the within-regime and between-regime SW amount feed-  
621 back maps are 0.33 on average across models, with an across-model standard  
622 deviation of 0.20. For the optical depth component, the pattern correlation  
623 is  $0.46 \pm 0.16$ . Hence while in some cases clouds of a given morphology may  
624 experience a large enough cloud property change that the resulting feedback  
625 is classified as between-regime rather within-regime, this does not appear to  
626 be a common occurrence.

### 627 3.5 SW cloud feedback contributions from individual regimes

628 The SW cloud feedback and its components presented above are computed by  
629 summing across all 8 regimes. We can gain further insights into the processes  
630 contributing to these feedbacks by considering the contributions to the feed-  
631 back from individual regimes. With the exception of Regime 1, the total SW  
632 cloud feedback is positive equatorward of about 50 degrees in all regimes, then  
633 becomes strongly negative in the extratropics, with a minimum at around 60  
634 degrees (Figure 9a). Similar to the maps shown in Figure 8, these features are  
635 closely mimicked by the between-regime component (Figure 9b), whereas the  
636 within-regime component is uniformly positive in nearly all regimes and all  
637 latitudes except poleward of about 55 degrees latitude (Figure 9c).

638 The amount and optical depth sub-components of the between-regime feed-  
639 back are shown in column 2 of Figure 9. Nearly everywhere, these two com-  
640 ponents act in the same direction, which makes sense because regimes with  
641 thicker-than-average clouds tend to be those with larger-than-average cloud  
642 cover (Table 2), so a given change in RFO causes both sub-components to  
643 have the same feedback sign. For regimes characterized by thicker-than-average  
644 clouds and more extensive cloud cover (Regimes 2, 5, and 8), increased RFO in  
645 the extratropics (see Figure 6b) causes negative SW cloud amount and optical  
646 depth feedback contributions, and decreased RFO at lower latitudes causes  
647 positive contributions (Figure 9e,h). For regimes characterized by thinner-  
648 than-average clouds and less extensive cloud cover (Regimes 3 and 6), increased  
649 RFO at low latitudes causes *positive* SW cloud amount and optical depth feed-  
650 back contributions, while decreased RFO in the extratropics causes *negative*  
651 contributions (Figure 9e,h). The overall features of the between-regime com-  
652 ponent suggest a tendency for the cloud population to shift from cloudier  
653 and thicker regimes (Regimes 2, 5, 8) towards less-cloudy and thinner regimes  
654 (Regimes 3 and 6) at low latitudes, with the opposite response in the extra-  
655 tropics. This leads to an overall between-regime SW cloud feedback that is

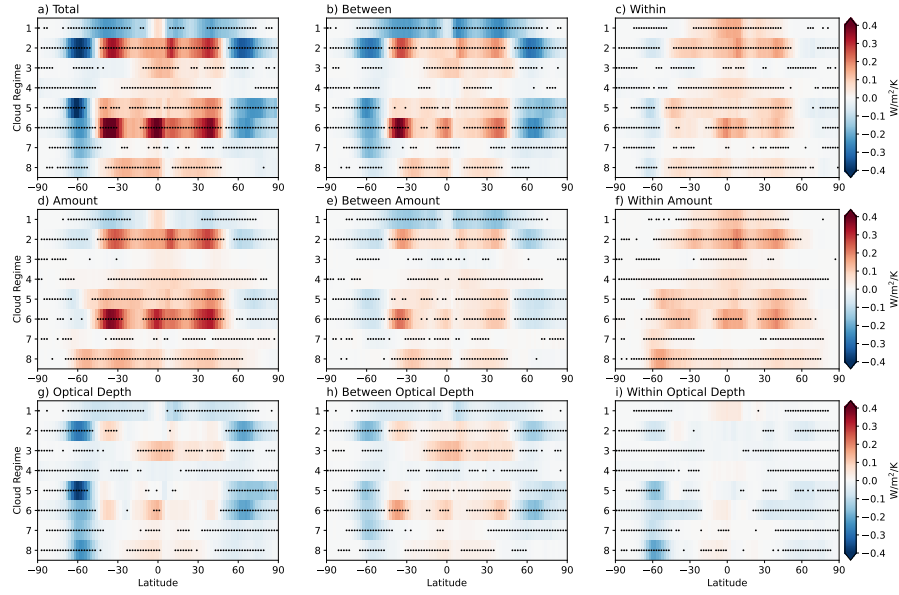


**Fig. 9** As in Figure 8, but showing the zonal mean contributions to the SW cloud feedback from each cloud regime. Stippling indicates locations where at least 8 out of 10 models agree on the sign of the change.

positive at low latitudes and negative at high latitudes (Figure 9b). Below we will show that this basic pattern holds across all models.

Figure 9 column 3 shows the feedbacks from changes in cloud properties within the already-present regimes. As shown previously, not only are the global mean within-regime components uniform in sign across models, but their geographic distributions are also nearly uniform in sign, with substantial inter-model agreement. In Figure 9f and i we can see that this uniformity extends to regime space. That is, cloud amount *within all individual regimes and at all latitudes* decreases with warming, particularly equatorward of about 60 degrees (Figure 9f). Similarly, cloud optical depth increases with warming *within all individual regimes poleward of about 40 degrees latitude* (Figure 9i). Hence, despite the wide diversity of cloud types and geographic distributions among the 8 regimes, they exhibit remarkably similar behavior in all regimes in response to warming: Clouds decrease in coverage at all latitudes and increase in albedo in the extratropics, causing positive amount and negative optical depth feedbacks, respectively.

3.6 SW cloud feedback contributions from individual models and between model generations

We now examine the zonal mean SW cloud feedback contributions in each of the ten individual models. The contributions to cloud feedback across all

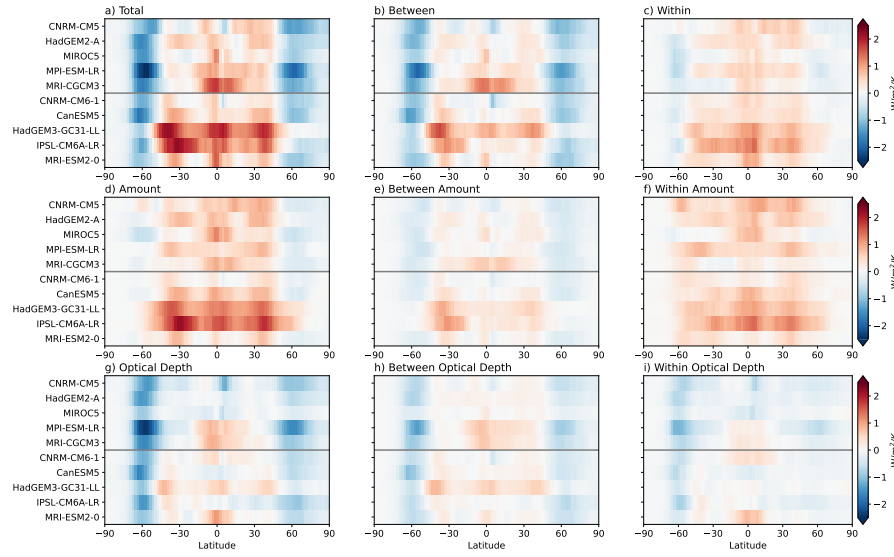


**Fig. 10** As in Figure 8, but showing the zonal mean contributions to the SW cloud feedback from each model. Horizontal line separates CMIP5 models (above) from CMIP6 models (below).

676 individual models agree qualitatively with the multi-model mean responses  
 677 discussed previously, with inter-model differences primarily occurring in the  
 678 relative magnitude of the responses as opposed to fundamental differences in  
 679 geographic structure. For example, all models indicate a positive low-latitude  
 680 feedback transitioning to a negative high-latitude feedback, with the former  
 681 coming primarily from the amount component and the latter coming from  
 682 the optical depth component. Previously we showed that the within-regime  
 683 amount component is systematically positive across latitude and regime for  
 684 the multi-model mean, and across all models for the global mean. We now see  
 685 in Figure 10f that it is systematically positive *across all models and latitudes*  
 686 as well. Similarly, Figure 10i confirms that the within-regime optical depth  
 687 feedback is systematically negative at high latitudes *across all models*, with  
 688 inter-model differences in sign at lower latitudes.

689 The extratropical SW cloud feedback has shifted towards stronger positive  
 690 or weaker negative values between CMIP5 and CMIP6, which is a key driver  
 691 of the increased climate sensitivity of these models (Zelinka et al., 2020). In  
 692 the smaller subset of models considered here, we see this manifest in weaker  
 693 negative feedbacks at high latitudes and stronger positive feedbacks at lower  
 694 latitudes in the CMIP6 models (Figure 11a). Consistent with Zelinka et al  
 695 (2020), both the amount and optical depth feedbacks contribute to the shift,  
 696 most dramatically in the extratropics (Figure 11d,g). The latitude range expe-  
 697 riencing positive amount and optical depth feedbacks has expanded poleward  
 698 in CMIP6, most notably in HadGEM3-GGC31-LL and IPSL-CM6A-LR (Fig-  
 699 ure 10a,d,g).

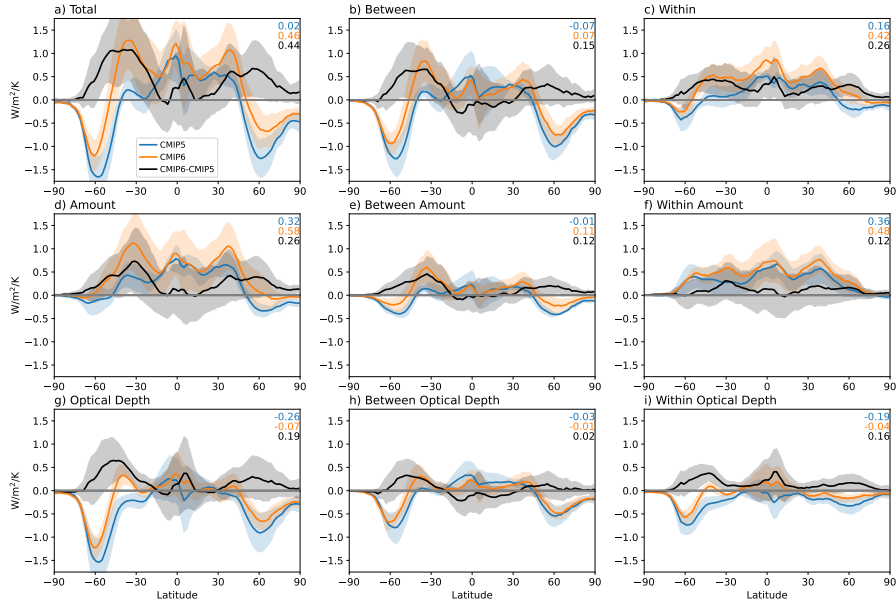


**Fig. 11** Zonal mean contributions to the SW cloud feedback, averaged across CMIP5 (blue) and CMIP6 (orange) models. Solid lines represent the multi-model means and the shading spans the  $\pm 1\sigma$  range across models. The difference between ensemble means is shown in black, with the shading representing the combined uncertainty from summing the individual ensembles'  $1\sigma$  ranges in quadrature. Global mean values are shown in the top right.

Whereas the within-regime component has shifted towards more positive values at all latitudes (Figure 11c), this shift is confined mostly to the extratropics for the between-regime component (Figure 11b). The shift of the within-regime component is primarily coming from a systematically stronger positive / weaker negative optical depth component (Figure 11i), with a smaller contribution from a stronger positive amount component (Figure 11f). The shift towards a weaker negative optical depth feedback in CMIP6 is consistent with a weaker cloud phase feedback owing to improved mean-state cloud phase in CMIP6 (Tan et al., 2016; McCoy et al., 2015). While this represents a shift towards better agreement with the broader body of evidence that this feedback is not strongly negative (Sherwood et al., 2020; Zelinka et al., 2022), it remains uncertain whether the improved mean-state necessarily means the latest models are better capturing all the physics needed for this feedback (Müllmenstädt et al., 2021).

The more-positive extratropical between-regime component in CMIP6 appears to receive roughly equal contributions from the amount and optical depth components (Figure 11e, h). The notable large increase around 30–50°S is related to a much larger increase in the RFO of Regime 6 – which has the thinnest and least extensive cloud coverage (not shown). In this same region, the cloudier/thicker Regime 5 decreases in CMIP6, whereas it increases in

720 CMIP5 (not shown). At higher latitudes, the negative between-regime component has become weaker. This is because of a weaker increase in the RFO of cloudier/thicker Regimes 2 and 5 and a weaker decrease in the RFO of less-cloudy/thinner Regimes 6 and 7 in CMIP6 (not shown). Hence the shift away from thinner and less extensive cloud regimes towards thicker and more extensive cloud regimes at high latitudes is more muted in CMIP6, whereas the shift towards thinner / less extensive cloud types at lower latitudes is a bit stronger in CMIP6. Both of these contribute to a more positive extratropical cloud feedback from between-regime shifts in CMIP6.

## 729 4 Conclusions and Discussion

730 In this study we have brought together for the first time two diagnostic strategies that offer complementary information about the processes causing the 731 cloud feedback. One, cloud radiative kernel analysis, allows for quantifying 732 the cloud feedback arising from changes in cloud amount, altitude, and optical 733 depth with warming. The other, cloud regime analysis, allows for determination 734 of the feedback from changes in cloud properties within distinct cloud 735 regimes separately from the feedback from changes in the relative occurrence 736 frequencies of various cloud regimes. Having first presented the mathematical 737 basis for combining these techniques, we then presented novel insights 738 about the cloud feedback that arise from applying the analysis to ten models 739 from CMIP5 and CMIP6 simulating a uniform 4K increase in sea surface tem- 740 perature. The analysis is performed for both longwave and shortwave cloud 741 feedback but for brevity we focused herein on the shortwave cloud feedback 742 results.

743 For any given model, both the within-regime and between-regime cloud 744 feedback components can be substantial. However, their roles are rather dif- 745 ferent: In the global average, the between-regime components tend to exhibit 746 substantial inter-model spread but a negligible ensemble-mean contribution. 747 Their geographic structures, however, largely determine the spatial pattern of 748 the total SW cloud feedback. These patterns reflect the fact that thinner, less 749 extensive cloud types increase at the expense of thicker, more extensive cloud 750 types at low latitudes, with the opposite response at high latitudes, leading to 751 an overall positive between-regime component at low latitudes and negative 752 between-regime component at high latitudes.

753 In contrast, the global mean within-regime components tend to be of uni- 754 form sign across models (systematically positive for cloud amount and nearly 755 systematically negative but of weaker magnitude for cloud optical depth), 756 such that they are the primary contributor to the positive ensemble-mean 757 SW cloud feedback. Their spatial patterns are very homogeneous, with near- 758 uniform positive contributions from cloud amount decreases and near-uniform 759 weaker negative contributions from cloud albedo increases.

760 Results are highly consistent when we perform the same analysis but with 761 the models' clouds matched to the 11 MODIS cloud regimes of Cho et al

(2021) rather than the 8 ISCCP cloud regimes of Tselioudis et al (2021), as shown in the Supplementary Information. One quantitative difference is that the ensemble mean between-regime amount component increases in strength slightly relative to those shown here (compare Figure 8e with SI Figure 2e), and the within-regime amount component decreases in strength slightly (compare Figure 8f with SI Figure 2f). This is unsurprising, as the likelihood of a location being reclassified to a different cloud regime in a warmed climate increases as the number of regimes increases, owing to the necessarily more subtle inter-regime differences in cloud properties when more regimes are present. It remains the case, however, that the ensemble mean between-regime feedback is near zero and the within-regime feedback is by far the dominant contributor to the overall feedback (compare Figure 7 with SI Figure 1). This indicates that our overall qualitative results are insensitive to the choice of observational cloud regimes to which the model fields are assigned.

Substantial model-to-model variations in the between-regime cloud feedback component are likely tied to variations in how large-scale meteorology – and the cloud regimes that it (dis)favors – changes with warming. However, these changes are not systematic across models, so the multi-model mean between-regime feedback is near zero. In contrast, very consistent feedbacks from temperature-mediated decreases in cloud coverage and increases in cloud optical depth are revealed once the obfuscating effects of changing large-scale meteorology are removed. The latter result is true even when considering individual cloud regimes, which exhibit systematic changes at all latitudes.

The negative optical depth feedback over the Southern Ocean receives contributions from both the increased frequency of occurrence of thicker cloud types relative to thinner cloud types, as well as increases in the albedo of clouds of a given morphology. This means that changes in meteorology that determine cloud morphology as well as thermodynamic processes that affect cloud reflectivity within a given meteorological condition are important.

CMIP6 models exhibit weaker negative feedbacks at high latitudes and stronger positive feedbacks at lower latitudes than their predecessors in CMIP5, consistent with previous work (Zelinka et al, 2020; Flynn and Mauritsen, 2020). Both cloud amount and optical depth feedbacks contribute to this shift, most dramatically in the extratropics. Within regimes, the decrease of cloud amount is greater in CMIP6, while the increase in cloud albedo is weaker in CMIP6, possibly related to increased mean-state supercooled liquid fractions that weaken the phase feedback. Additionally, the increased frequency of thicker/cloudier regimes at high latitudes is less dramatic in CMIP6, while the shift towards thinner/less-cloudy regimes at lower latitudes is more dramatic, both of which contribute to a more positive between-regime extratropical feedback in CMIP6.

To the extent that internal climate variability and long-term greenhouse warming lead to distinct changes in large-scale circulation, whereas the response of cloud properties to warming within meteorological regimes is timescale-invariant, future work should investigate whether across-timescale correspondence of cloud feedback improves if considering only the within-regime compo-

809 nent. If so, this could provide an effective strategy for constraining a portion  
810 of cloud feedback, especially in regions where changes in large-scale meteorol-  
811 ogy or model biases in control-climate meteorology (Kelleher and Grise, 2022)  
812 may obscure the otherwise close relationship between temperature-mediated  
813 changes in cloud properties of a given morphology across time scales.

814 **Acknowledgements** We acknowledge the World Climate Research Programme, which,  
815 through its Working Group on Coupled Modelling, coordinated and promoted CMIP. We  
816 thank the climate modeling groups for producing and making available their model output,  
817 the Earth System Grid Federation (ESGF) for archiving the data and providing access,  
818 and the multiple funding agencies who support CMIP and ESGF. We thank Daeho Jin for  
819 guidance with normalization and Yoko Tsushima, Karl Taylor, and Steve Klein for useful  
820 discussions.

## 821 References

- 822 Barnes EA, Polvani L (2013) Response of the Midlatitude Jets, and of Their  
823 Variability, to Increased Greenhouse Gases in the CMIP5 Models. *Journal*  
824 *of Climate* 26(18):7117–7135, DOI 10.1175/jcli-d-12-00536.1
- 825 Bodas-Salcedo A, Williams KD, Field PR, Lock AP (2012) The Surface Down-  
826 welling Solar Radiation Surplus over the Southern Ocean in the Met Of-  
827 fice Model: The Role of Midlatitude Cyclone Clouds. *Journal of Climate*  
828 25(21):7467–7486, DOI 10.1175/jcli-d-11-00702.1
- 829 Bodas-Salcedo A, Williams KD, Ringer MA, Beau I, Cole JNS, Dufresne  
830 JL, Koshiro T, Stevens B, Wang Z, Yokohata T (2014) Origins of  
831 the Solar Radiation Biases over the Southern Ocean in CFMIP2 Mod-  
832 els. *Journal of Climate* 27(1):41–56, DOI 10.1175/JCLI-D-13-00169.  
833 1, URL [https://journals.ametsoc.org/view/journals/clim/27/1/  
834 jcli-d-13-00169.1.xml](https://journals.ametsoc.org/view/journals/clim/27/1/jcli-d-13-00169.1.xml), publisher: American Meteorological Society Sec-  
835 tion: *Journal of Climate*
- 836 Bony S, Dufresne JL (2005) Marine boundary layer clouds at the heart of  
837 tropical cloud feedback uncertainties in climate models. *Geophys Res Lett*  
838 32, DOI 10.1029/2005GL023851
- 839 Bony S, Lau KM, Sud YC (1997) Sea Surface Temperature and Large-Scale  
840 Circulation Influences on Tropical Greenhouse Effect and Cloud Radiative  
841 Forcing. *J Climate* 10:2055–2077, DOI 10.1175/1520-0442(1997)0102.0.CO;  
842 2
- 843 Bony S, Dufresne JL, Treut HL, Morcrette JJ, Senior C (2004) On dynamic  
844 and thermodynamic components of cloud changes. *Climate Dyn* 22:71–68,  
845 DOI 10.1007/s00382-003-0369-6
- 846 Bony S, Stevens B, Coppin D, Becker T, Reed KA, Voigt A, Medeiros B (2016)  
847 Thermodynamic control of anvil cloud amount. *Proceedings of the National*  
848 *Academy of Sciences* DOI 10.1073/pnas.1601472113
- 849 Boucher O, Servonnat J, Albright AL, Aumont O, Balkanski Y, Bastrikov V,  
850 Bekki S, Bonnet R, Bony S, Bopp L, Braconnot P, Brockmann P, Cadule  
851 P, Caubel A, Cheruy F, Codron F, Cozic A, Cugnet D, D’Andrea F, Davini

- 852 P, Lavergne Cd, Denvil S, Deshayes J, Devilliers M, Ducharne A, Dufresne  
853 JL, Dupont E, Éthé C, Fairhead L, Falletti L, Flavoni S, Foujols MA,  
854 Gardoll S, Gastineau G, Ghattas J, Grandpeix JY, Guenet B, Guez L  
855 E, Guilyardi E, Guimberteau M, Hauglustaine D, Hourdin F, Idelkadi A,  
856 Joussaume S, Kageyama M, Khodri M, Krinner G, Lebas N, Levavasseur  
857 G, Lévy C, Li L, Lott F, Lurton T, Luyssaert S, Madec G, Madeleine  
858 JB, Maignan F, Marchand M, Marti O, Mellul L, Meurdesoif Y, Mignot  
859 J, Musat I, Ottlé C, Peylin P, Planton Y, Polcher J, Rio C, Rochetin N,  
860 Rousset C, Sepulchre P, Sima A, Swingedouw D, Thiéblemont R, Traore  
861 AK, Vancoppenolle M, Vial J, Vialard J, Viovy N, Vuichard N (2020)  
862 Presentation and Evaluation of the IPSL-CM6A-LR Climate Model. *Journal  
863 of Advances in Modeling Earth Systems* 12(7):e2019MS002,010,  
864 DOI 10.1029/2019MS002010, URL <https://agupubs.onlinelibrary.wiley.com/doi/abs/10.1029/2019MS002010>,  
865 \_eprint: <https://agupubs.onlinelibrary.wiley.com/doi/pdf/10.1029/2019MS002010>
- 866 Cho N, Tan J, Oreopoulos L (2021) Classifying Planetary Cloudiness with  
867 an Updated Set of MODIS Cloud Regimes. *Journal of Applied Meteorology  
868 and Climatology* 60(7):981–997, DOI 10.1175/JAMC-D-20-0247.1,  
869 URL <https://journals.ametsoc.org/view/journals/apmc/aop/JAMC-D-20-0247.1.xml>, publisher: American  
870 Meteorological Society Section: Journal of Applied Meteorology and Climatology
- 871 Collins WJ, Bellouin N, Doutriaux-Boucher M, Gedney N, Hinton PHT,  
872 Hughes J, Jones CD, Joshi M, Liddicoat S, Martin G, O'Connor F, Rae  
873 J, Senior C, Sitch S, Totterdell I, Wiltshire A, Woodward S (2011) Develop-  
874 ment and evaluation of an Earth-system model - HadGEM2. *Geosci Model  
875 Dev Discuss* 4:997–1062
- 876 Del Genio AD, Wolf AB (2000) The temperature dependence of the liquid  
877 water path of low clouds in the southern Great Plains. *Journal of Climate*  
878 13(19):3465–3486, DOI 10.1175/1520-0442(2000)013<3465:ttdotl>2.0.co;2
- 879 Eitzen ZA, Xu KM, Wong T (2011) An Estimate of Low-Cloud Feedbacks  
880 from Variations of Cloud Radiative and Physical Properties with Sea Surface  
881 Temperature on Interannual Time Scales. *Journal of Climate* 24(4):1106–  
882 1121, DOI 10.1175/2010jcli3670.1
- 883 Eyring V, Bony S, Meehl GA, Senior CA, Stevens B, Stouffer RJ, Tay-  
884 lor KE (2016) Overview of the Coupled Model Intercomparison Project  
885 Phase 6 (CMIP6) experimental design and organization. *Geosci Model Dev*  
886 9(5):1937–1958, DOI 10.5194/gmd-9-1937-2016
- 887 Flynn CM, Mauritsen T (2020) On the climate sensitivity and his-  
888 torical warming evolution in recent coupled model ensembles. *Atmo-  
889 spheric Chemistry and Physics* 20(13):7829–7842, DOI <https://doi.org/10.5194/acp-20-7829-2020>, URL <https://acp.copernicus.org/articles/20/7829/2020/>
- 890 Gordon ND, Klein SA (2014) Low-cloud optical depth feedback in climate  
891 models. *Journal of Geophysical Research-Atmospheres* 119(10):6052–6065,  
892 DOI 10.1002/2013jd021052
- 893
- 894
- 895
- 896

- 897 Gordon ND, Norris JR (2010) Cluster analysis of midlatitude oceanic cloud  
898 regimes: mean properties and temperature sensitivity. *Atmospheric Chemistry and Physics* 10(13):6435–6459, DOI 10.5194/acp-10-6435-2010
- 899 Gordon ND, Norris JR, Weaver CP, Klein SA (2005) Cluster analysis of cloud  
900 regimes and characteristic dynamics of midlatitude synoptic systems in  
901 observations and a model. *Journal of Geophysical Research-Atmospheres*  
902 110(D15), DOI 10.1029/2004jd005027
- 903 Jakob C, Tselioudis G (2003) Objective identification of cloud  
904 regimes in the Tropical Western Pacific. *Geophysical Research Letters* 30(21), DOI  
905 10.1029/2003GL018367, URL <https://onlinelibrary.wiley.com/doi/abs/10.1029/2003GL018367>, eprint:  
906 <https://onlinelibrary.wiley.com/doi/pdf/10.1029/2003GL018367>
- 907 Jin D, Oreopoulos L, Lee D (2017a) Regime-based evaluation of cloudiness  
908 in CMIP5 models. *Climate Dynamics* 48(1):89–112, DOI 10.1007/  
909 s00382-016-3064-0, URL <https://doi.org/10.1007/s00382-016-3064-0>
- 910 Jin D, Oreopoulos L, Lee D (2017b) Simplified ISCCP cloud regimes for  
911 evaluating cloudiness in CMIP5 models. *Climate Dynamics* 48(1):113–  
912 130, DOI 10.1007/s00382-016-3107-6, URL <https://doi.org/10.1007/s00382-016-3107-6>
- 913 Kelleher MK, Grise KM (2022) Varied midlatitude shortwave cloud  
914 radiative responses to Southern Hemisphere circulation shifts. *Atmospheric Science Letters* 23(1):e1068, DOI  
915 10.1002/asl.1068, URL <https://onlinelibrary.wiley.com/doi/abs/10.1002/asl.1068>,  
916 eprint: <https://onlinelibrary.wiley.com/doi/pdf/10.1002/asl.1068>
- 917 Klein SA, Jakob C (1999) Validation and sensitivities of frontal clouds sim-  
918 ulated by the ECMWF model. *Mon Weath Rev* 127:2514–2531, DOI  
919 10.1175/1520-0493(1999)1272.0.CO;2
- 920 Klein SA, Hall A, Norris JR, Pincus R (2017) Low-Cloud Feedbacks from  
921 Cloud-Controlling Factors: A Review. *Surveys in Geophysics* DOI 10.1007/  
922 s10712-017-9433-3
- 923 McCoy DT, Hartmann DL, Zelinka MD, Ceppi P, Grosvenor DP (2015) Mixed-  
924 phase cloud physics and Southern Ocean cloud feedback in climate models.  
925 *Journal of Geophysical Research-Atmospheres* 120(18):9539–9554, DOI 10.  
926 1002/2015jd023603
- 927 McCoy DT, Field PR, Elsaesser GS, Bodas-Salcedo A, Kahn BH, Zelinka MD,  
928 Kodama C, Mauritzen T, Vanniere B, Roberts M, Vidale PL, Saint-Martin  
929 D, Volodire A, Haarsma R, Hill A, Shipway B, Wilkinson J (2019) Cloud  
930 feedbacks in extratropical cyclones: insight from long-term satellite data  
931 and high-resolution global simulations. *Atmospheric Chemistry and Physics*  
932 19(2):1147–1172, DOI 10.5194/acp-19-1147-2019
- 933 McCoy DT, Field P, Bodas-Salcedo A, Elsaesser GS, Zelinka MD (2020) A  
934 Regime-Oriented Approach to Observationally Constraining Extratropical  
935 Shortwave Cloud Feedbacks. *Journal of Climate* 33(23):9967–9983, DOI  
936 10.1175/JCLI-D-19-0987.1, URL <https://journals.ametsoc.org/view/journals/clim/33/23/jcliD190987.xml>
- 937
- 938
- 939
- 940
- 941

- 942 Myers TA, Norris JR (2016) Reducing the uncertainty in subtropical cloud  
943 feedback. *Geophysical Research Letters* 43(5):2144–2148, DOI 10.1002/  
944 2015gl067416
- 945 Myers TA, Scott RC, Zelinka MD, Klein SA, Norris JR, Caldwell PM  
946 (2021) Observational constraints on low cloud feedback reduce uncer-  
947 tainty of climate sensitivity. *Nature Climate Change* 11(6):501–507, DOI  
948 10.1038/s41558-021-01039-0, URL <https://www.nature.com/articles/s41558-021-01039-0>, number: 6 Publisher: Nature Publishing Group
- 949 Mülmenstädt J, Salzmann M, Kay JE, Zelinka MD, Ma PL, Nam C, Kret-  
950 zschmar J, Hörnig S, Quaas J (2021) An underestimated negative cloud  
951 feedback from cloud lifetime changes. *Nature Climate Change* 11(6):508–  
952 513, DOI 10.1038/s41558-021-01038-1, URL <https://www.nature.com/articles/s41558-021-01038-1>, number: 6 Publisher: Nature Publishing  
953 Group
- 954 Norris JR, Iacobellis SF (2005) North Pacific cloud feedbacks inferred from  
955 synoptic-scale dynamic and thermodynamic relationships. *Journal of Cli-  
956 mate* 18(22):4862–4878, DOI 10.1175/jcli3558.1
- 957 Oreopoulos L, Rossow WB (2011) The cloud radiative effects of International  
958 Satellite Cloud Climatology Project weather states. *Journal of Geophysical  
959 Research-Atmospheres* 116, DOI 10.1029/2010jd015472
- 960 Rossow W, Walker A, Beuschel D, Roiter M (1996) International Satel-  
961 lite Cloud Climatology Project (ISCCP) Documentation of New Cloud  
962 Datasets. WMO/TD-No 737, World Meteorological Organization p 115 pp
- 963 Sherwood SC, Webb MJ, Annan JD, Armour KC, Forster PM, Harg-  
964 reaves JC, Hegerl G, Klein SA, Marvel KD, Rohling EJ, Watanabe  
965 M, Andrews T, Braconnot P, Bretherton CS, Foster GL, Hausfather Z,  
966 Heydt ASvd, Knutti R, Mauritsen T, Norris JR, Proistosescu C, Ru-  
967 genstein M, Schmidt GA, Tokarska KB, Zelinka MD (2020) An Assess-  
968 ment of Earth’s Climate Sensitivity Using Multiple Lines of Evidence. *Re-  
969 views of Geophysics* 58(4):e2019RG000,678, DOI <https://doi.org/10.1029/2019RG000678>, URL <https://agupubs.onlinelibrary.wiley.com/doi/abs/10.1029/2019RG000678>
- 970 Soden BJ, Broccoli AJ, Hemler RS (2004) On the use of cloud forc-  
971 ing to estimate cloud feedback. *J Climate* 17:3661–3665, DOI 10.1175/  
972 1520-0442(2004)0172.0.CO;2
- 973 Soden BJ, Held IM, Colman R, Shell KM, Kiehl JT, Shields CA (2008) Quanti-  
974 fying Climate Feedbacks Using Radiative Kernels. *J Climate* 21:3504–3520,  
975 DOI 10.1175/2007JCLI2110.1
- 976 Stevens B, Giorgetta M, Esch M, Mauritsen T, Crueger T, Rast S, Salzmann  
977 M, Schmidt H, Bader J, Block K, Brokopf R, Fast I, Kinne S, Kornblueh L,  
978 Lohmann U, Pincus R, Reichler T, Roeckner E (2013) Atmospheric compo-  
979 nent of the MPI-M Earth System Model: ECHAM6. *Journal of Advances  
980 in Modeling Earth Systems* 5(2):146–172, DOI 10.1002/jame.20015
- 981 Swart NC, Cole JNS, Kharin VV, Lazare M, Scinocca JF, Gillett NP,  
982 Anstey J, Arora V, Christian JR, Hanna S, Jiao Y, Lee WG, Majaess  
983 F, Saenko OA, Seiler C, Seinen C, Shao A, Sigmond M, Solheim L, von  
984

- 988 Salzen K, Yang D, Winter B (2019) The Canadian Earth System Model  
989 version 5 (CanESM5.0.3). *Geoscientific Model Development* 12(11):4823–  
990 4873, DOI 10.5194/gmd-12-4823-2019, URL <https://gmd.copernicus.org/articles/12/4823/2019/>, publisher: Copernicus GmbH
- 991 Tan I, Storelvmo T, Zelinka MD (2016) Observational constraints on mixed-  
992 phase clouds imply higher climate sensitivity. *Science* 352(6282):224–227,  
993 DOI 10.1126/science.aad5300
- 994 Taylor KE, Stouffer RJ, Meehl GA (2012) An Overview of CMIP5 and the  
995 Experiment Design. *Bull Amer Meteor Soc* 93(4):485–498, DOI 10.1175/  
996 BAMS-D-11-00094.1
- 997 Terai CR, Klein SA, Zelinka MD (2016) Constraining the low-cloud optical  
998 depth feedback at middle and high latitudes using satellite observations.  
1000 *Journal of Geophysical Research-Atmospheres* 121(16):9696–9716, DOI 10.  
1001 1002/2016jd025233
- 1002 Tselioudis G, Rossow WB (2006) Climate feedback implied by observed ra-  
1003 diation and precipitation changes with midlatitude storm strength and fre-  
1004 quency. *Geophysical Research Letters* 33(2), DOI 10.1029/2005gl024513
- 1005 Tselioudis G, Rossow WB, Rind D (1992) Global Patterns of Cloud Optical  
1006 Thickness Variation with Temperature. *J Climate* 5:1484–1495, DOI 10.  
1007 1175/1520-0442(1992)0052.0.CO;2
- 1008 Tselioudis G, Rossow WB, Jakob C, Remillard J, Tropf D, Zhang Y (2021)  
1009 Evaluation of Clouds, Radiation, and Precipitation in CMIP6 Models  
1010 Using Global Weather States Derived from ISCCP-H Cloud Property Data.  
1011 *Journal of Climate* 34(17):7311–7324, DOI 10.1175/JCLI-D-21-0076.1,  
1012 URL <https://journals.ametsoc.org/view/journals/clim/aop/JCLI-D-21-0076.1/JCLI-D-21-0076.1.xml>, publisher: American Meteo-  
1013 rological Society Section: Journal of Climate
- 1014 Tsushima Y, Ringer MA, Webb MJ, Williams KD (2013) Quantitative eval-  
1015 uation of the seasonal variations in climate model cloud regimes. *Climate*  
1016 *Dynamics* 41(9):2679–2696, DOI 10.1007/s00382-012-1609-4, URL <https://doi.org/10.1007/s00382-012-1609-4>
- 1017 Tsushima Y, Ringer MA, Koshiro T, Kawai H, Roehrig R, Cole J, Watan-  
1018 abe M, Yokohata T, Bodas-Salcedo A, Williams KD, Webb MJ (2016)  
1019 Robustness, uncertainties, and emergent constraints in the radiative re-  
1020 spondences of stratocumulus cloud regimes to future warming. *Climate Dy-  
1021 namics* 46(9):3025–3039, DOI 10.1007/s00382-015-2750-7, URL <https://doi.org/10.1007/s00382-015-2750-7>
- 1022 Voldoire A, Saint-Martin D, Sénési S, Decharme B, Alias A, Chevallier M,  
1023 Colin J, Guérémy JF, Michou M, Moine MP, Nabat P, Roehrig R, Méliá  
1024 DSy, Séférian R, Valcke S, Beau I, Belamari S, Berthet S, Cassou C,  
1025 Cattiaux J, Deshayes J, Douville H, Ethé C, Franchistéguy L, Geoffroy O,  
1026 Lévy C, Madec G, Meurdesoif Y, Msadek R, Ribes A, Sanchez-Gomez E,  
1027 Terray L, Waldman R (2019) Evaluation of CMIP6 DECK Experiments  
1028 With CNRM-CM6-1. *Journal of Advances in Modeling Earth Systems*  
1029 11(7):2177–2213, DOI 10.1029/2019MS001683, URL <https://agupubs.onlinelibrary.wiley.com/doi/abs/10.1029/2019MS001683>, \_eprint:  
1030
- 1031
- 1032
- 1033

- 1034 <https://agupubs.onlinelibrary.wiley.com/doi/pdf/10.1029/2019MS001683>
- 1035 Watanabe M, Suzuki T, Oishi R, Komuro Y, Watanabe S, Emori S, Take-  
1036 mura T, Chikira M, Ogura T, Sekiguchi M, Takata K, Yamazaki D,  
1037 Yokohata T, Nozawa T, Hasumi H, Tatebe H, Kimoto M (2010) Im-  
1038 proved Climate Simulation by MIROC5: Mean States, Variability, and  
1039 Climate Sensitivity. *Journal of Climate* 23(23):6312–6335, DOI 10.1175/  
1040 2010JCLI3679.1, URL <https://journals.ametsoc.org/view/journals/clim/23/23/2010jcli3679.1.xml>, publisher: American Meteorological So-  
1041 ciety Section: Journal of Climate
- 1042 Webb M, Senior C, Bony S, Morcrette JJ (2001) Combining ERBE and ISCCP  
1043 data to assess clouds in the Hadley Centre, ECMWF and LMD atmospheric  
1044 climate models. *Climate Dyn* 17:905–922, DOI 10.1007/s003820100157
- 1045 Williams K, Tselioudis G (2007) GCM intercomparison of global cloud  
1046 regimes: present-day evaluation and climate change response. *Climate Dyn*  
1047 29:231–250, DOI 10.1007/s00382-007-0232-2
- 1048 Williams K, Webb M (2009) A quantitative performance assessment of  
1049 cloud regimes in climate models. *Climate Dyn* 33:141–157, DOI 10.1007/  
1050 s00382-008-0443-1
- 1051 Williams KD, Copsey D, Blockley EW, Bodas-Salcedo A, Calvert D,  
1052 Comer R, Davis P, Graham T, Hewitt HT, Hill R, Hyder P, Ineson  
1053 S, Johns TC, Keen AB, Lee RW, Megann A, Milton SF, Rae JGL,  
1054 Roberts MJ, Scaife AA, Schiemann R, Storkey D, Thorpe L, Wat-  
1055 terson IG, Walters DN, West A, Wood RA, Woollings T, Xavier PK  
1056 (2018) The Met Office Global Coupled Model 3.0 and 3.1 (GC3.0 and  
1057 GC3.1) Configurations. *Journal of Advances in Modeling Earth Systems*  
1058 10(2):357–380, DOI 10.1002/2017MS001115, URL <https://agupubs.onlinelibrary.wiley.com/doi/abs/10.1002/2017MS001115>, \_eprint:  
1059 <https://agupubs.onlinelibrary.wiley.com/doi/pdf/10.1002/2017MS001115>
- 1060 Yin JH (2005) A consistent poleward shift of the storm tracks in simulations  
1061 of 21st century climate. *Geophys Res Lett* 32, DOI 10.1029/2005GL023684
- 1062 Yukimoto S, Adachi Y, Hosaka M, Sakami T, Yoshimura H, Hirabara M,  
1063 Tanaka TY, Shindo E, Tsujino H, Deushi M, Mizuta R, Yabu S, Obata A,  
1064 Nakano H, Koshiro T, Ose T, Kitoh A (2012) A New Global Climate Model  
1065 of the Meteorological Research Institute: MRI-CGCM3—Model Description  
1066 and Basic Performance—. *Journal of the Meteorological Society of Japan*  
1067 Ser II 90A:23–64, DOI 10.2151/jmsj.2012-A02
- 1068 Yukimoto S, Kawai H, Koshiro T, Oshima N, Yoshida K, Urakawa S, Tsu-  
1069 jino H, Deushi M, Tanaka T, Hosaka M, Yabu S, Yoshimura H, Shindo E,  
1070 Mizuta R, Obata A, Adachi Y, Ishii M (2019) The Meteorological Research  
1071 Institute Earth System Model Version 2.0, MRI-ESM2.0: Description and  
1072 Basic Evaluation of the Physical Component. *Journal of the Meteorological*  
1073 *Society of Japan Ser II* 97(5):931–965, DOI 10.2151/jmsj.2019-051
- 1074 Zelinka M (2021) mzzelinka/cloud-radiative-kernels: Sep 17, 2021 Release. DOI  
1075 10.5281/zenodo.5514137, URL <https://zenodo.org/record/5514137>
- 1076 Zelinka MD, Hartmann DL (2011) The observed sensitivity of high clouds to  
1077 mean surface temperature anomalies in the tropics. *Journal of Geophysical*  
1078

- 1080 Research-Atmospheres 116, DOI 10.1029/2011JD016459  
1081 Zelinka MD, Klein SA, Hartmann DL (2012a) Computing and Partitioning  
1082 Cloud Feedbacks Using Cloud Property Histograms. Part I: Cloud Radiative  
1083 Kernels. *Journal of Climate* 25(11):3715–3735, DOI 10.1175/jcli-d-11-00248.  
1084 1  
1085 Zelinka MD, Klein SA, Hartmann DL (2012b) Computing and Partitioning  
1086 Cloud Feedbacks Using Cloud Property Histograms. Part II: Attribution to  
1087 Changes in Cloud Amount, Altitude, and Optical Depth. *Journal of Climate*  
1088 25(11):3736–3754, DOI 10.1175/JCLI-D-11-00249.1  
1089 Zelinka MD, Klein SA, Taylor KE, Andrews T, Webb MJ, Gregory JM, Forster  
1090 PM (2013) Contributions of Different Cloud Types to Feedbacks and Rapid  
1091 Adjustments in CMIP5. *Journal of Climate* 26(14):5007–5027, DOI 10.1175/  
1092 jcli-d-12-00555.1  
1093 Zelinka MD, Zhou C, Klein SA (2016) Insights from a refined decomposition  
1094 of cloud feedbacks. *Geophysical Research Letters* 43(17):9259–9269, DOI  
1095 10.1002/2016gl069917  
1096 Zelinka MD, Myers TA, McCoy DT, Po-Chedley S, Caldwell PM, Ceppi P,  
1097 Klein SA, Taylor KE (2020) Causes of Higher Climate Sensitivity in CMIP6  
1098 Models. *Geophysical Research Letters* 47(1):e2019GL085782, DOI <https://doi.org/10.1029/2019GL085782>, URL <https://agupubs.onlinelibrary.wiley.com/doi/abs/10.1029/2019GL085782>  
1099  
1100 Zelinka MD, Klein SA, Qin Y, Myers TA (2022) Evaluating Climate Models' Cloud Feedbacks Against Expert  
1101 Judgment. *Journal of Geophysical Research: Atmospheres* 127(2):e2021JD035198, DOI 10.1029/2021JD035198, URL <https://onlinelibrary.wiley.com/doi/abs/10.1029/2021JD035198>, \_eprint:  
1102 <https://onlinelibrary.wiley.com/doi/pdf/10.1029/2021JD035198>  
1103  
1104 Zhang Y, Klein SA (2013) Factors Controlling the Vertical Extent  
1105 of Fair-Weather Shallow Cumulus Clouds over Land: Investigation of  
1106 Diurnal-Cycle Observations Collected at the ARM Southern Great  
1107 Plains Site. *Journal of the Atmospheric Sciences* 70(4):1297–1315, DOI  
1108 10.1175/JAS-D-12-0131.1, URL <https://journals.ametsoc.org/view/journals/atsc/70/4/jas-d-12-0131.1.xml>, publisher: American Meteorological Society Section: Journal of the Atmospheric Sciences  
1109  
1110  
1111  
1112  
1113

## 1114 Declarations

- 1115 – **Funding:** MDZ, IT, and LO are were supported by NASA grant 80NSSC18K1599.  
1116 MDZ's work was additionally supported by the U.S. Department of Energy (DOE) Regional and Global Modeling Analysis program area and  
1117 was performed under the auspices of the DOE by Lawrence Livermore National Laboratory under Contract DE-AC52-07NA27344. LO and GT were  
1118 additionally supported by the NASA MEaSUREs program.  
1119 – **Conflict of interest/Competing interests:** The authors have no relevant  
1120 financial or non-financial interests to disclose.

- 
- 1123 – **Ethics approval:** Not applicable
  - 1124 – **Consent to participate:** Not applicable
  - 1125 – **Consent for publication:** Not applicable
  - 1126 – **Availability of data and materials:** ISCCP HGG weather states are  
1127 available at <https://isccp.giss.nasa.gov/wstates/hggws.html>. Cloud  
1128 radiative kernels are available at <https://doi.org/10.5281/zenodo.5514137>  
1129 (Zelinka, 2021).
  - 1130 – **Code availability:** Python code to perform all calculations and produce  
1131 all figures and tables in this manuscript will be made available in a GitHub  
1132 repository, for which a doi will be registered before final publication.
  - 1133 – **Authors' contributions:** All authors contributed to the study conception  
1134 and design. Data analysis was performed by MDZ. The first draft of  
1135 the manuscript was written by MDZ and all authors commented on subse-  
1136 quent versions of the manuscript. All authors read and approved the final  
1137 manuscript.

## Supplementary Files

This is a list of supplementary files associated with this preprint. Click to download.

- [Zelinkaetal20220415SI.pdf](#)